Epidemic Financing Facilities: Pandemic Bonds and Endemic Swaps

Shimeng Huang[a], Ken Seng Tan[b*], Jinggong Zhang[b], Wenjun Zhu[b†]

[a]Department of Risk and Insurance, Wisconsin School of Business

University of Wisconsin-Madison, USA

[b]Division of Banking & Finance, Nanyang Business School

Nanyang Technological University, Singapore

Abstract

While the COVID-19 pandemic has shattered the world with severe human toll and catastrophic economic losses and sufferings, it has also heightened the need for more effective solutions for managing epidemic-related risks. This paper proposes two capital market-based epidemic financing facilities to address two extremes of epidemic risks. The proposed pandemic bond is meant to hedge the severe pandemic outbreak, while the proposed endemic swap can be used to hedge a recurrent endemic. Using coronavirus as an example of a pandemic and dengue fever as an example of an endemic, we discuss the modeling and pricing of the proposed epidemic securities. We price the proposed securities based on epidemiological models and actuarial models. We show that the proposed hedging securities can provide additional capital relief for pandemic recovery plans, effectively stabilize hedgers' cash flows, and create attractive returns for different investors.

Keywords: Securitization, Pandemic bond, Endemic swap, Coronavirus, Dengue
JEL codes: G19 · G22 · G32 · H12

---

*We are deeply saddened that Professor Ken Seng Tan left us on January 1, 2023.

†Corresponding author. E-mail: wjzhu@ntu.edu.sg.

"By connecting investments to sustainability goals and by ensuring transparency, issuers and investors can help in the fight against the pandemic and shape a more resilient and sustainable future for all."

- Anshula Kant, Managing Director and CFO of the World Bank Group

August 14, 2020

1 Introduction

Since its initial outbreak in December 2019, the highly contagious COVID-19 infection has spread rapidly around the globe. As of the end of 2021, it has infected more than 295 million individuals and led to more than 5.49 million deaths worldwide.[1] The global pandemic has also significantly disrupted economic activities. The International Monetary Fund estimated that the cumulative loss to global GDP from COVID-19 could be US$9 trillion from 2020 to 2021. Moreover, research shows that globalization and the dual phenomena of climate change and urbanization have exacerbated and intensified epidemic risks (Bloom et al., 2018; Hilsenrath, 2020). This raises the important question: How could societies achieve more effective epidemic risk transfer and risk sharing?

Similar to catastrophe risks, pandemic risks are characterized by low frequency and high severity (Gründl et al., 2021). Cummins et al. (2002) show that catastrophe risk diversification in the insurance industry might not be sufficient. Market imperfections, such as moral hazard and adverse selection problems (Niehaus, 2002), as well as price regulation (Froot, 2001) limit sufficient catastrophe risk sharing. Thus, low-frequency and high-severity risks can be diversified in the financial market through risk securitization (Charpentier, 2008; Cummins and Trainar, 2009; Doherty, 1997). Another major challenge pertaining to epidemic risk management is that epidemics can lead to large accumulations of losses. Especially when an epidemic spreads rapidly and affects multiple countries around the world simultaneously, it is impossible to be diversified and eliminated through traditional insurance risk pooling. Cummins (2006) concludes that cataclysmic events with a significant impact on global capital markets are globally undiversifiable. Moreover, losses from a pandemic are likely to span a long time. This means moral hazard, both internal and external, can be an issue (Richter and Wilson, 2020). Therefore, private insurers' appetite for pandemic risk is limited, and most recent pandemic risk insurance proposals require backstops from governments.[2] Indeed, some researchers study the insurability of pandemic risk and share the view that pandemic risk may not be insurable by the insurance industry alone (Gründl et al., 2021), and may lead to failure of the private pandemic insurance market (Hartwig et al., 2020; Richter and Wilson, 2020).

[1] Source: `https://www.worldometers.info/coronavirus/`

[2] See Table 1 of OECD for a list of recent pandemic risk insurance proposals from different countries and insurance societies.

Transferring systemic risk via securitization and financial innovation has been popular in the past few decades.[3] Closely related to our work, MacMinn and Richter (2018) compare indemnity-based triggers and index-based triggers in designing insurance-linked securities to hedge excess mortality risk in a shareholder value maximization framework. Pandemic event is one important reason that causes excess mortality. Excess mortality risk due to pandemic event is similar to the property risk associated with catastrophic events. In our paper, we focus on securitizing *pandemic risks*, which goes beyond mortality risk and has very limited discussion in the literature. The pandemic risk differs from the mortality risk in two important ways. First, apart from mortality shocks, pandemic risk exposure also includes medical expenditure and economic relief funds. Second, pandemic risk has low predictability and high severity. Hence, a severe pandemic event can be highly costly to governments. Thus, our paper focuses on hedging pandemic risks from governments' viewpoint and explores the modeling of pandemic risk, different pandemic bond designs, and their pricing framework. Like a CAT bond, a pandemic bond can be developed with payouts contingent on pandemic occurrences and their severities. In 2017, the World Bank launched a first-ever pandemic bond to support its $500 million Pandemic Emergency Financing Facility (PEF). The PEF has been criticized for its overly stringent criteria for releasing funds and its slow and complicated mechanism. This pandemic bond was not renewed when it expired in July 2020. No other pandemic bonds have been issued. Nevertheless, seeking capital market solutions to pandemic risks is still important. It has great potential due to the systemic nature of pandemic risks and the much larger capital base in the financial market compared to the commercial (re)insurance industry.[4]

Just like other natural catastrophes, the *occurrence* of an epidemic event is independent of the financial market. Thus, investors may use epidemic securities to diversify their investment and reap potentially satisfactory returns during an economic downturn. Therefore, pandemic securities can be an attractive alternative to investors, as highlighted in a recent report by Lloyd's that "*capital market participants may have the appetite to underwrite products that offer protection against future pandemics; at the same time customer demand has increased significantly.*" Motivated by the World Bank PEF and other responses to COVID-19, in this paper, we aim to develop epidemic securitization structures that are more transparent and that can respond to dramatic epidemic events more promptly. Our proposed securitization schemes focus on two types of epidemic risk, i.e., pandemic risk

[3] A wide range of categories of systemic risks have become securitized, including catastrophic (CAT) risks (e.g., Braun, 2016; Cummins et al., 2004; Cummins and Weiss, 2009; Finken and Laux, 2009; Härdle and Cabrera, 2010; Huang et al., 2023), weather derivatives (e.g., Brockett et al., 2009; 2005; Chen et al., 2023; Ito et al., 2016; Woodard and Garcia, 2008; Zhang et al., 2019; Zhu et al., 2018), mortality and longevity risks (e.g., Blake et al., 2013; Blake and Cairns, 2020; Denuit et al., 2007; Dowd et al., 2006; Li et al., 2017; Lin and Cox, 2007; Tan et al., 2022; Zhu et al., 2017). See Cowley and Cummins (2005) for securitization of life insurance assets and liabilities.

[4] It is estimated that the global commercial (re)insurance market's total capital base is around $2 trillion. In contrast, the capacity of the capital markets is about $180 trillion (Lloyd's, 2020).

and endemic risk. Broadly speaking, a pandemic is an epidemic outbreak that has spread over multiple countries or continents. The frequency of pandemic risk is low, but the economic damage from a pandemic can be catastrophic. In contrast, an endemic is a recurrent disease with a persistent presence within a specific geographic area. For example, Figure 1, which depicts the number of dengue cases in Singapore over the period 1990-2020 (WHO, 2017; MOH Singapore, 2019; NEA Singapore, 2020), demonstrates that the dengue fever is a recurrent event, and the annual exposure to the dengue cases can be highly uncertain. The high volatility of the exposure to endemic risk raises considerable concern for insurers underwriting dengue insurance. In this paper, we propose to use pandemic bonds to hedge the former risk and the endemic swaps for the latter risk.

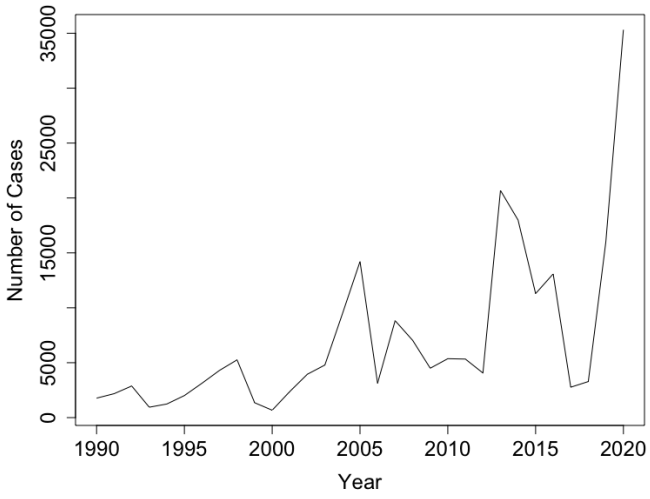


Figure 1: Number of annual dengue cases in Singapore for the period 1990-2020

In the empirical analysis of this paper, we discuss the modeling and pricing of the proposed epidemic securities, using coronavirus as an example of pandemic and dengue fever as an example of endemic. The basic susceptible-infected-removed (SIR) model was first developed by Kermack and McKendrick (1927). In this model, individuals are classified into three stages - susceptible (S), infectious (I), and removed (R). This basic SIR model has been developed and extended since 1927 with the inclusion of more stages to account for different characteristics of various infectious diseases. Feng and Garrido (2011) explore the SIR model in actuarial modeling to calculate insurance premiums and reserves. They argue that epidemiological models capture the dynamics of infectious diseases and dependence between insurance payers and beneficiaries better than traditional actuarial models. In our empirical analysis, we extend the original deterministic SIR model to a stochastic version following Jia and Tsui (2005). Using data from the U.S, we use the stochastic SIR model

to simulate coronavirus cases.

The SIR model is also useful in modeling diseases whose transmissions are not only human-to-human, such as the dengue virus, which has vector-to-human transmission. We extend the deterministic periodic-forced SIR-SEI model (Andraud et al., 2013) to a stochastic model and allow increasing human and vector populations over time. We fit the model to weekly dengue data in Singapore.[5] The empirical results show that the proposed securities can provide additional capital for pandemic recovery plans and effectively stabilize hedgers' cash flows.

COVID-19 mutations such as Delta and Omicron may escape immunity and lead to reinfections (Eggink et al., 2021; Karim and Karim, 2021; Townsend et al., 2021). Therefore, in this paper, we also adapt our stochastic SIR model to include the impact of reinfection (Malkov, 2020; Zhai et al., 2021). In addition, vaccines and antiviral medications have been developed at an unprecedented speed and have played a vital role in the fight against COVID-19. For example, the Pfizer-BioNTech COVID-19 Vaccine has been available under Emergency Use Authorization (EUA) since December 11, 2020. Pfizer's Paxlovid, the first oral COVID-19 antiviral treatment, was approved under EUA on December 22, 2021. Therefore, we also account for the effects of vaccination and antiviral controls (De la Sen and Ibeas, 2021). We find that the proposed pandemic bond can provide similarly satisfying hedging performance in these extensions.

This paper contributes to the literature mainly in the following ways. First, we propose several epidemic financing facility designs. Epidemic securities are still very new in the market. The first and only pandemic bond issued in history, the World Bank PEF, has been heavily criticized for its complicated and slow mechanism. Our proposed pandemic bond designs directly address the criticism with simpler and more transparent structures. They can respond to dramatic epidemic events in a more timely fashion. The proposed structures and their pricing results provide insights into the feasibility and effectiveness of epidemic financing facilities in risk mitigation. Second, this paper prices the proposed securities by combining epidemiological and actuarial models. To the best of our knowledge, this is the first paper in actuarial science literature that employs a stochastic epidemiological model which incorporates complicated effects such as reinfections and vaccination in actuarial modeling and pricing. The article provides guidance in future epidemic financing facilities development.

The rest of this paper proceeds as follows. Section 2 summarizes current epidemic financing

[5]Epidemiological modeling is not the focus of this research, therefore, in this paper, we focus on basic models. There are many variations of the basic SIR model. For example, an extended SIR model distinguishes symptomatic and asymptomatic patients (Giordano et al., 2020), and a SEIR model and its extensions add an exposed (E) state into the model (e.g., Allen, 2017; Lin et al., 2020; Raza et al., 2019). For dengue fever, researchers also use SIRSI models (Chanprasopchai et al., 2018; Derouich and Boutayeb, 2006; Perera, 2019).

facilities in the market. Section 3 introduces the structures of the pandemic bond and the endemic swap proposed and their pricing framework. Section 4 presents an empirical analysis. A coronavirus bond and a dengue swap are priced using stochastic simulations of future coronavirus and dengue cases. Section 5 presents sensitivity tests. Section 6 concludes the paper.

2 Current Epidemic Risk Solutions

Pandemic Emergency Financing Facility (PEF)

The PEF was issued by the World Bank in 2017 (International Bank for Reconstruction and Development, 2017a). It is a financing facility designed to rapidly mobilize funding from the international community to contain a pandemic outbreak. It aims to fill the financing gap after the initial outbreak of pandemics and before large-scale humanitarian relief assistance is available. The PEF was set up for three years, from July 2017 to June 2020.

The PEF covers six types of diseases – flu, coronavirus, filovirus, Lassa fever virus, Rift Valley fever virus, and Crimean Congo Hemorrhagic fever virus. It consists of a cash window and an insurance window, which have different sources of funds and different mechanisms for releasing funds. The cash window is financed entirely by donors with no private sector involvement, and funds are allocated when criteria for the insurance window are not met. In the insurance window, a pandemic bond and insurance is sold to institutional investors and reinsurance companies. Premiums and coupons are paid to private investors and reinsurers by donors through the World Bank Group treasury. Upon activation of the insurance window, i.e., the trigger to release the fund and reduce coupon and/or principal payout is met, the partial or full amount of the insurance window fund is paid to International Development Association (IDA) eligible countries – the recipients of the risk coverage.

Central Emergency Response Fund (CERF)

The CERF[6] that was launched by the United Nations comprises of three windows - CERF loans, Underfunded Emergencies, and Rapid Response. CERF loans lend money to eligible humanitarian organizations at the beginning of an emergency. CERF Underfunded Emergencies allocate grants to selected countries to support humanitarian response activities and sudden-onset emergencies or rapidly deteriorating conditions in an existing emergency. CERF rapid response funds can help to reduce the inconsistency and delays that humanitarian organizations may experience when receiving voluntary contributions. These funds are disbursed immediately after a disaster and must be expended within six months.

[6]Details are available at: `https://cerf.un.org`.

Country-based Pool Funds (CBPF)

The CBPF[7] launched by the United Nations allows donors to pool their contributions into single, unearmarked funds to support local humanitarian efforts. This enables humanitarian partners in crisis-affected countries to deliver timely, coordinated, and principled assistance.

Contingency Fund for Emergencies (CFE)

The CFE[8] launched by the World Health Organization (WHO) provides resources to respond immediately to disease outbreaks and humanitarian crises with health consequences. The ability to respond quickly - in as little as 24 hours - before other funding is mobilized can stop a health emergency from spiraling out of control, saving lives and resources. WHO has released nearly $9 million from the CFE in response to COVID-19 to support preparedness and response activities in the most vulnerable countries with weak health systems.

Epidemic Insurance

Traditionally the market for epidemic insurance has been very small. There is dengue insurance which provides insurance cover for endemic risks related to dengue fever. Such insurance is quite popular in South East Asia. On the other hand, there are very few insurance coverages for pandemics. In fact, it is a common practice to exclude pandemic risks from insurance covers. Most property damage policies only cover business interruptions due to physical damage and exclude communicable diseases. In 2017, Munich Re started to provide customized risk transfer solutions for all business interruptions due to the epidemic. The coverage includes business interruption, delay in start-up, temporary site closure, etc. Munich Re also launched PathogenRX cover in 2018, the first insurance solution of its kind to provide financial protection against an infectious disease outbreak. While there was hardly any demand for such insurance cover before 2020, inquiries for PathogenRX surged after the COVID-19 outbreak (Collins, 2020). In response to COVID-19, some insurers and risk management entities have started to develop programs to cover pandemic-related business losses. For example, the Insurance Services Office in the United States develops endorsements for commercial property policies covering business interruption losses due to COVID-19-related business closures (OECD, 2020). The Lloyd's proposes several systemic risk management frameworks in response to the COVID-19 crisis, including ReStart, RecoverRe, Black Swan Re, and calls for public-private partnership. European Insurance and Occupational Pensions Authority (EIOPA) also encourages risk sharing between insurers,

[7]Details are available at: `https://www.unocha.org/our-work/humanitarian-financing/country-based-pooled-funds-cbpf`.

[8]Details are available at: `https://www.who.int/emergencies/funding/contingency-fund-for-emergencies`.

reinsurers, and governments at the national or European level.

Critiques on the Current Epidemic Risk Solutions

While financial facilities such as the CERF Rapid Response window, CBPF, and the CFE, can respond very quickly to emergencies by releasing funds immediately after a disaster occurs, their drawback is that they rely entirely on a donor-based mechanism and hence, are facing re-financing issues. In contrast, the PEF draws funds from capital markets rather than relying entirely on voluntary contributions. The PEF, however, has been criticized for being slow in releasing the fund due to its stringent criteria and complicated mechanism. For example, the EBOLA outbreak in the Democratic Republic of the Congo (DRC), which has claimed more than 2000 lives since 2018, failed to trigger the insurance window of the PEF because the activation criterion of at least 20 deaths in a second country (other than the DRC) was not met. The COVID-19 crisis activated the PEF insurance window only on Apr 17, 2020, more than three months after the initial outbreak of the global pandemic in December 2019. This is because triggering the insurance window needs to satisfy both a minimum waiting period of 12 weeks and a minimum rolling cases growth rate.

Insurance companies have limited capacity to cover pandemic risks due to the systemic nature of the risk. The American Property Casualty Insurance Association estimates that U.S. insurers' risk capital would have been drained within weeks if coronavirus-related business interruption losses had been covered. Munich Re argues that such risks are uninsurable by the private sector alone and urges the creation of state-backed risk pools to make pandemic risks acceptable. Insurers and industry associations, such as EIOPA, also call for government intervention in covering pandemic risks.

A pandemic bond issued by governments or global organizations could be a viable option to transfer the uninsurable pandemic risk from the insurance sector to capital markets. It could resolve the sustainability issue by relying on the capital market while not depending on the donors' funds. To address the issues with the PEF, simpler and more transparent structures are required to make the hedging instruments more responsive to pandemic emergencies like COVID-19.

3 Proposed Securitization for Epidemic Risk

Next subsection presents several securitization structures that could be used to hedge pandemic and endemic risks while Subsection 3.2 discusses their pricing.

3.1 Epidemic Securitization Structure

From a hedging point of view, it is important to distinguish the type of epidemic. A pandemic is defined as a large-scale epidemic that has spread over several countries or con-

tinents, affecting a large number of people (e.g., COVID-19 and EBOLA). The frequency of pandemic risk is low, but the economic damage from a pandemic can be enormous. A pandemic bond can be attractive to interrupted individuals, corporations, and governments to transfer pandemic risks to capital market. In contrast, an endemic is defined as an ongoing disease with a persistent presence within a geographic area (e.g., seasonal flu and dengue fever). For endemic risk, we propose to use a swap arrangement to hedge a stream of future contingent liabilities.[9] The pandemic bond is discussed in Subsection 3.1.1 and an endemic swap is proposed in Subsection 3.1.2. For ease of reference, Table 1 summarises the variables that will be used in both structures.

Table 1: Definitions of variables that are used in the proposed pandemic bond and endemic swap structures

Variable	**Definition**
V	Price of the pandemic bond
n	Term to maturity
x	First trigger level in the pandemic bond
y	Second trigger level in the pandemic bond
b	Maximum coupon payout of the pandemic bond for period t
B_t	Actual coupon payout of the pandemic bond for period t
f	Face value / maximum principal payout of the pandemic bond upon maturity
F	Actual principal payout of the pandemic bond upon maturity
CC_t	Cumulative number of pandemic cases at time t $(0 < t \leq n)$
$RC_t^{(p)}$	Maximum rolling pandemic cases in period t with rolling period p
	$RC_1^{(p)} = \max_{s \in (p,1]} (CC_s - CC_{s-p})$
	$RC_t^{(p)} = \max_{s \in (t-1,t]} (CC_s - CC_{s-p})$ for $t = 2, 3, \ldots, n$
C	Fixed payment of the endemic swap
NC_t	Number of new endemic cases in period t
D_t	Floating payment of the endemic swap for period t
	D_t is directly proportional to NC_t at $\$q$ per case, i.e. $D_t = q \times NC_t$

[9]Both bonds and swaps with appropriate designs can potentially be used to mitigate different types of epidemic risk. However, the recurring cash flows naturally make swaps more suitable for recurrent endemic events with high frequency yet low severity. In contrast, the significantly reduced liabilities of contingent bonds during pandemic events are generally more appropriate for hedging pandemic risk with low frequency but high severity losses. In addition, a bond issuer can collect capital upfront to respond to future high-severity losses more promptly. On the contrary, in response to low-severity losses, it may not be necessary to prepare for large loss reserving upfront.

3.1.1 Pandemic Bond Structure

In a catastrophe (CAT) bond, the bond coupon and/or principal payments are contingent on whether a pre-defined catastrophic trigger event has been met (see, e.g., (Braun, 2016; Cummins, 2008; Cummins and Trainar, 2009)). As pandemic events have low frequency and high severity like other natural catastrophes, we propose pandemic bonds to address such risks. A pandemic bond is similar to a CAT bond with payouts (coupons and principal) contingent on some well-specified pandemic events. Under normal circumstances, i.e., without any pandemic events, the pandemic bond is just like the conventional bonds involving regular coupon payments at a regular schedule and principal repayment at maturity. When a pandemic strikes with its severity triggering a pre-defined threshold, the bond payouts to the investors will be reduced or stopped. The reduction in the bond payouts can then be used by the bond issuer to fund the costs arising from pandemic events. The pandemic bond, therefore, exposes investors to pandemic risk in exchange for a higher potential risk premium.

CAT bonds are popular in the market for their high yields and low correlations with the returns from the financial market. Therefore, they are attractive to investors as a financial tool for risk diversification purposes (Braun, 2016; Cummins, 2008). Just like natural catastrophes, the *occurrence* of an epidemic event is independent of the financial market. Indeed, upon a preliminary examination, we find that pandemic risks tend to have low correlations with the financial market. More specifically, we calculate the correlation coefficients between 14-day rolling confirmed COVID-19 cases in the U.S., from the 14th day to the $(366 - \ell)$th day of 2020, and S&P 500 daily returns, from the $(14+\ell)$th day to the 366th day of 2020, where $\ell = 0, 1, 2, ...,$ is the number of lagged days. Figure 2 displays the calculated correlations against different ℓ values. For ℓ smaller than 23 days, the correlations are positive; for ℓ between 23 and 60 days, the correlations are negative. In addition, the magnitudes of correlations are consistently low, and the negative correlation starts to bounce back after around 40 lagged days. This is consistent with the market observation that the stock market soon recovered after the initial plunge of stock prices after the COVID-19 outbreak (McKinsey & Company, 2021). This correlation calculation exercise provides direct evidence that securities written on pandemic risk can potentially induce diversification benefits to their investors' portfolios.

The bond issuers, which can be governments, global organizations and cooperatives (e.g., the World Bank), insurers, reinsurers, and corporations, can either issue pandemic bonds directly or via a special purpose vehicle (SPV). SPV pools assets from different operating entities and sells bonds to different tranches of investors. One important advantage of SPV is that it reduces the issuer's default risk. Pandemic risks that we discuss in this paper can be globally undiversifiable. Thus, government interventions are essential.[10] Therefore,

[10]Taking COVID-19 as an example, we have observed huge expenses borne by the government since its outburst, including providing medical and emergency operations and supplies, setting up and maganing

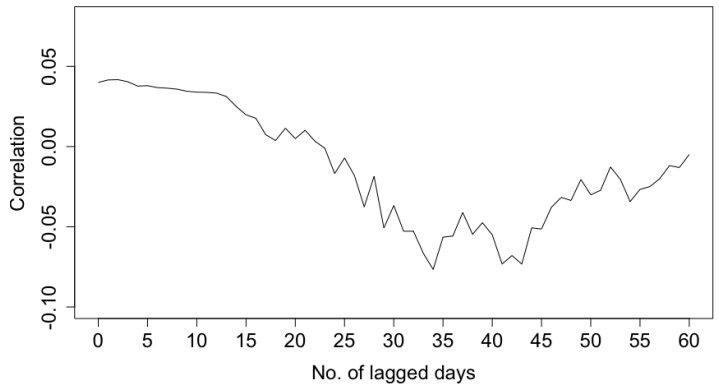


Figure 2: Overall correlations of COVID-19 and S&P500 daily returns in 2020

in this paper, we limit the bond issuers to governments and global organizations in our discussion. Since governments and global organizations rarely default, the default risk can be ignored, and we simplify the framework of bond issuance by assuming no SPV involved, i.e., the bond issuer sells the pandemic bond directly to investors.

The issuer collects premiums upfront and pays coupons and principal to investors. Suppose the bond is designed to mature at the end of year n. Investors first pay a fixed bond premium V at the inception of the bond. In return, the bond issuer pays investors annual coupons at the end of each year and the principal value upon maturity of the bond. The coupons and principal amount may be reduced if a pandemic occurs during the bond's term to maturity. We focus on the economic losses related to pandemic risks, which are the primary concern of governments and global organizations. Therefore, we choose rolling confirmed cases as our trigger, which is directly related to economic losses in the region. Another reason for using rolling confirmed cases is to address PEF's problems of stringent criteria and complicated trigger mechanisms because the data of rolling cases are easy to calculate and are readily available in a timely fashion.

In this subsection, we consider both fixed principal (FP) and variable principal (VP) designs, which entail different levels of risk and thus, could be of interest to investors with different risk appetites. The two structures outlined both have a binary reduction design – the coupon or principal payout is immediately reduced to zero once the trigger is reached. In Online Appendix A, we also consider linear reduction designs of coupon or principal payouts – the coupon or principal payout is linearly reduced to zero after the trigger is met.

quarantine and stay-home notice facilities, acting swiftly in procuring goods and services, offering direct transfers and loans to eligible businesses and households, etc. For example, in 2020, the Singapore government's commitment to supporting the economy and society in fighting the COVID-19 pandemic was $72.2 billion, which was over 20% of its GDP in 2020.

It is shown that the pricing results for the binary reduction designs and linear reduction designs are similar. Thus, we will focus on fixed principal and variable principal structures with binary reduction in the main results of this paper.

Design FP - Binary Coupon and Fixed Principal (BCFP)

In a BCFP structure, the bond pays investors a fixed principal value of f upon bond maturity and contingent annual coupons B_t of value b if the rolling cases stay below the fixed trigger level x throughout the year, i.e., $RC_t^{(p)} < x$, with p to be the length of the rolling window. At any time during the year, if the rolling cases reach x, i.e., $RC_t^{(p)} \geq x$, coupon payment for the year is immediately reduced to zero. More specifically, coupon payout in period t is

$$B_t = \begin{cases} 0, \text{ if } RC_t^{(p)} \geq x, \\ b, \text{ if } RC_t^{(p)} < x. \end{cases} \tag{1}$$

Design VP - Binary Coupon and Binary Principal (BCBP)

In a BCBP design, we impose two layers of triggers, x and y, and also allow the face value to be affected by pandemic risk. The second layer, y, is designed to be much larger than the first layer, x, providing higher protection in global pandemic events such as COVID-19. Similar to BCFP, the coupon payout B_t depends on whether $RC_t^{(p)}$ exceeds the first trigger level x. In addition to the first layer trigger, if $RC_t^{(p)}$ reaches the second trigger level y, all future payouts, including both the principal, F, and future coupons, are reduced to zero. Coupon payout in period t for the BCBP design is

$$B_t = \begin{cases} 0, & \text{if } \max\limits_{1\leq s\leq t}\{RC_s^{(p)}\} \geq y \text{ or } x \leq RC_t^{(p)} < y, \\ b, & \text{if } \max\limits_{1\leq s\leq t-1}\{RC_s^{(p)}\} < y \text{ and } RC_t^{(p)} < x, \end{cases} \tag{2}$$

and principal payout upon maturity is

$$F = \begin{cases} 0, \text{ if } \max\limits_{1\leq t\leq n}\{RC_t^{(p)}\} \geq y, \\ f, \text{ if } \max\limits_{1\leq t\leq n}\{RC_t^{(p)}\} < y. \end{cases} \tag{3}$$

3.1.2 Endemic Swap Structure

As pointed out earlier in Figure 1 that endemic such as dengue fever exposes insurers that underwrite fever insurance to endemic liabilities. While the endemic is a recurrent

infectious disease, its severity varies significantly from year to year, and so do the insurers' endemic liabilities. The recurrent but uncertain severity of the endemic exposure suggests that a swap with its floating payments proportional to the number of endemic disease cases can be a viable hedging instrument for the insurers to covert their uncertain endemic payments into a series of fixed payments. This is precisely our motivation in proposing the endemic swap with the insurers taking the floating-receiver and fixed-payer position and the counterparty paying floating and receiving fixed. The counterparty investors can be pension funds, investment banks, mutual funds, and other institutional investors with the risk appetite to take the counterparty position in such a swap structure. More explicitly, hedgers with exposure to endemic liabilities pay fixed payments, C, in exchange for floating payments, D_t, through the endemic swap arrangement. The floating payments D_t are proportional to the number of endemic cases in period t. Note also that the swap arrangement does not require an initial cash outlay, and such a feature can be appealing to both hedgers and investors.

3.2 Pricing Framework

The standard approach to pricing contingent claim securities is based on the equivalent martingale approach. When the market is complete, there exists only one equivalent martingale (risk-neutral) probability measure, and the price of any contingent claim is simply its expected discounted payoff under the martingale measure. The epidemic financial facility market pertinent to this paper is incomplete since the underlying epidemic risk is not traded. In this case, there exists more than one equivalent martingale measure, leading to a range of no-arbitrage prices. Methods such as that based on minimizing quadratic hedging risk error, indifferent pricing, Essher Transform, etc., have been proposed. For simplicity, we consider the use of Wang's transform (Wang, 1996; 2000; 2002) to identify the equivalent martingale measure for pricing.

Let V be the price of a pandemic bond. Then V can be computed based on the expected discounted coupons and principal payouts under an equivalent martingale measure $\mathbb{Q}$-measure:

$$V = \mathsf{E}^{\mathbb{Q}}[F]d(0,n) + \sum_{t=1}^{n} \mathsf{E}^{\mathbb{Q}}\left[B_t\right] d(0,t), \tag{4}$$

where $d(0,t)$ is the (deterministic) discount rate for cash flow at time t.

For the endemic swap, we assume the frequency of payments is $1/m$ year. For example, $m = 2$ means payments are made semi-annually. The fixed payment C is determined at the inception of the swap contract such that both fixed and floating legs have the same

expected present value under an equivalent martingale measure $\mathbb{Q}$:

$$\sum_{t=1}^{mn} Cd\left(0, \frac{t}{m}\right) = \sum_{t=1}^{mn} \mathsf{E}^{\mathbb{Q}}\left[D_{t/m}\right] d\left(0, \frac{t}{m}\right), \tag{5}$$

where $\{D_{t/m}\}_{t=1,2,\ldots,mn}$ is the series of floating payments and $d\left(0, \frac{t}{m}\right)$ is the discount rate for cash flow at time t/m.

By using Wang's distortion risk measure that converts the distribution functions between the real-world probability measure $\mathbb{P}$ and a risk-neutral probability measure $\mathbb{Q}$,[11] the distorted (a.k.a. risk-adjusted) distribution, $F_t^{\mathbb{Q}}(u)$, for a given distribution $F_t(u)$ is

$$F_t^{\mathbb{Q}}(u) = \Phi\left[\Phi^{-1}(F_t(u)) - \lambda\right], \tag{6}$$

where Φ is the cumulative distribution function of the standard normal distribution and λ is a parameter representing the market price of risk. In pricing the pandemic bond, $F_t(u) = \mathsf{P}(RC_t^{(p)} \leq u)$ is the probability of $RC_t^{(p)}$ not reaching the trigger level $u \in \{x, y\}$ in period t; in pricing the endemic swap, $F_t(u) = \mathsf{P}(NC_t \leq u)$ is the cumulative distribution function of NC_t, the number of total new endemic cases in period t.

4 Empirical Analysis

In this section, we investigate two examples of the proposed epidemic financial facilities. In Subsection 4.1, we discuss coronavirus bonds to illustrate the pandemic bond designs. In Subsection 4.2, we take a dengue swap contract as an example of the endemic swap proposed in this paper.

4.1 Coronavirus Bond

4.1.1 Coronavirus Simulation Model

The coupon and principal payouts of a coronavirus bond depend on the occurrences and number of coronavirus cases within the bond's term to maturity. For human-to-human transmission diseases, the basic SIR model, first developed by Kermack and McKendrick (1927), remains popular and is widely used by researchers with variations and extensions. In actuarial applications, Feng and Garrido (2011) develop a framework for actuarial calculations using the SIR model. They suggest epidemiological models have advantages in modeling insurance coverage against infectious diseases over traditional actuarial models

[11] Wang transform has been widely used in pricing financial and insurance risks in incomplete markets. For example, it has been successfully applied to price mortality- and longevity- linked securities (see, e.g., Denuit et al., 2007; Lin and Cox, 2005; 2007).

such as life table methods and multistate models. In this paper, we construct the coronavirus rolling cases simulation by extending the original deterministic SIR model to a stochastic model discussed in Jia and Tsui (2005). The transmission process represented by the SIR model is displayed in Figure 3. We use $S(t)$, $I(t)$, and $R(t)$ to represent the number of susceptible, infectious, and removed (including recovered and dead) individuals at time t, respectively. Since pandemics usually do not last for more than ten years, births and deaths within the population are ignored in this model. Therefore, the total population, $N = S(t) + I(t) + R(t)$ remains constant in an SIR model. The deterministic transmission process is governed by the set of ordinary differential equations (ODE) (7) and parameters used in the SIR simulation are summarized in Table 2.

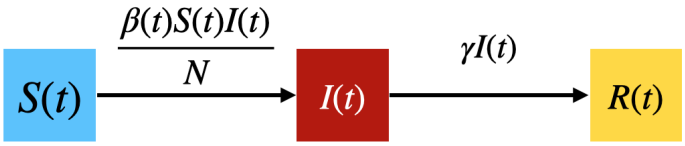


Figure 3: Pandemic SIR model

$$\begin{aligned} \frac{dS(t)}{dt} &= -\frac{\beta(t)S(t)I(t)}{N}, \\ \frac{dI(t)}{dt} &= \frac{\beta(t)S(t)I(t)}{N} - \gamma I(t), \\ \frac{dR(t)}{dt} &= \gamma I(t). \end{aligned} \tag{7}$$

The main challenges of estimating pandemic-related parameters stem from the inconsistency of raw data and the complex nature of epidemiological models (De la Sen and Ibeas, 2021). Some key parameter values, including the reproduction rate and daily removal rate, are well studied. There is a broad consensus about their values in the scientific community.[12] Since this paper focuses on the securitization of epidemic risks instead of epidemiological modeling, we adopt a parsimonious yet, widely used SIR model shown in Figure 3 and re-estimate some parameters using methods recommended in the literature.

Table 2 summarizes the parameter values. An important parameter in an SIR model is the reproduction rate, defined as the average number of adequate contacts (with both susceptible and other individuals) of an infectious individual during the infectious period.

[12]Studies that develop more complicated epidemiological models primarily focus on the formulation and mathematical properties of the models instead on parameters estimation (see, e.g., Eletreby et al., 2020; Malkov, 2020; Maurício de Carvalho and Moreira-Pinto, 2021; Sridhar et al., 2021; Zhai et al., 2021).

It is difficult to measure the reproduction number R_0 precisely due to limited data and incomplete reporting. The value of R_0 depends on country, culture, calculation methods, and model assumptions (Liu et al., 2020). IBRD (2017b) assumes R_0 follows a Gamma distribution with its rate and shape parameters being estimated from a dataset of past coronavirus events. This dataset, however, does not include an R_0 value from COVID-19. Some recent findings, such as that reported in Linka et al. (2020); Park et al. (2020), indicate that the estimated R_0 value of COVID-19 varies quite widely. In particular, among the 20 estimates of R_0 value of COVID-19 that are reviewed by Park et al. (2020), R_0 ranges from 1.9 to 6.5. For our applications, we take the mean of these 20 estimates, which can be deemed as the average reproduction number of COVID-19, and incorporate it into IBRD's (2017b) dataset. We then follow IBRD's (2017b) method and re-estimate the rate and shape parameters of the Gamma distribution with the updated dataset and find that R_0 follows a Gamma distribution, $\Gamma(7.076, 2.505)$.

According to the IBRD's (2017b) model on coronavirus in the PEF Prospectus, with active containment, the reproduction rate can be significantly reduced from the initial reproduction rate, R_0, to R_c, the reproduction rate after containment and the time until active containment, T_c, follows an exponential distribution with a mean of 156 days. Measures of active containment include government policies such as mask-wearing, social distancing, and stay-at-home order. These measures can effectively curb the spread of the virus and thus, reduce the reproduction rate significantly (Catching et al., 2021; Kwon et al., 2021; Wang et al., 2020). Moreover, it is generally believed that coronavirus infection leads to natural immunity.[13] In this SIR model, we follow the common assumption that infection gives permanent immunity. Thus, the "removed" state shown in Figure 3 is an absorbing state and there is no transition from $R(t)$ to $S(t)$. We relax this assumption in Section 5.1 by considering a model that captures the escape of immunity and reinfections.[14]

We solve the ODE using Euler's method with a step size of 1 day. Following Jia and Tsui (2005), in the stochastic extension, we assume that the number of people moving from state $S(t)$ to state $I(t)$ follows a Poisson distribution. The number of people moving from state

[13] Although there have been cases of positive retesting, whether reinfection from the same virus is possible remains a contentious issue (Costa et al., 2021; Falahi and Kenarkoohi, 2020). Researchers provide numerous reasons for positive retesting, including false-negative results at discharge, prolonged shedding/reactivation, increased virus replication due to discontinuation of the drug after clinical symptoms recovery (Gousseff et al., 2020; Tao et al., 2021), and dead viruses but viral genomic fragments (Kang et al., 2020).

[14] In our baseline analysis, we focus on the classic SIR structure and make the simplification that the "removed" state is absorbing. We do acknowledge the limitations of this model. For example, the COVID-19 virus has developed numerous mutations, such as the widespread Delta and Omicron variants in 2021. Research has shown that mutations could escape immunity and, therefore, lead to possible reinfections (Eggink et al., 2021; Karim and Karim, 2021; Townsend et al., 2021). Moreover, COVID-19 vaccinations and antiviral treatments have been developed to combat the virus. The SIR model formulated in Equation (7) can be easily modified to include these complications. Extended models with COVID-19 reinfection and antiviral controls will be discussed in Sections 5.1 and 5.2, respectively.

Table 2: SIR Model Parameters

Parameter	Definition	Value	Reference
$\beta(t)$	Daily contact rate	γR_0 or γR_c	Calculated
γ (day^{-1})	Daily removal rate	1/14	Baud et al. (2020); Bhapkar et al. (2020); Jia and Tsui (2005)
T_c (day^{-1})	Time until active containment	Exp(1/156)	IBRD (2017b)
R_0	Reproduction rate before T_c	$\Gamma(7.076, 2.505)$	Re-estimated based on IBRD (2017b) and Park et al. (2020)
$\mathsf{E}(R_c)$	Mean reproduction rate after T_c	0.57	IBRD (2017b)
N	The U.S. population	329.5 million	World Bank (2020)
$I(0)$	Initial index case	1	Jia and Tsui (2005)
$S(0)$	Initial susceptible individuals	$N-1$	Jia and Tsui (2005)
$R(0)$	Initial removed individuals	0	Jia and Tsui (2005)

$I(t)$ to state $R(t)$ follows a Binomial distribution. For the frequency model for coronavirus, following IBRD 's PEF Prospectus, we assume it follows a Poisson distribution with a mean of 1 event per 15 years. In other words, the waiting time between occurrences of successive events follows an exponential distribution with a mean of 15 years. Furthermore, we assume that no more than one coronavirus event can take place at the same time.

Details of the coronavirus simulation process, which involves three key steps, are presented in Algorithm 1. The rolling cases simulation (Step 1) generates the number of cases and event duration, and the frequency simulation (Step 2) gives coronavirus events starting time during the bond's term to maturity. 10,000 rounds of simulations are performed for both rolling cases and frequency.

4.1.2 Coronavirus Bond Pricing Results

A typical CAT bond covering risks such as storms, earthquakes, and floods usually has a term to maturity ranging from 1 year to 4 years, though 3 to 4 years are most common (Barrieu and Albertini, 2010; Polacek et al., 2018; Swiss Re, 2021). The World Bank PEF – the only pandemic bond to date – also has a term to maturity of 3 years. For this reason, in our empirical analysis, we similarly choose three years as our pandemic bond's term to maturity. Based on the experience of the ongoing pandemic, assuming a 3-year term to maturity seems appropriate as it can provide timely short-term financing for the pandemic while being reasonably long enough for economic recovery. We use Step 3 of Algorithm 1 to price a 3-year coronavirus bond. We set the value of the maximum

Algorithm 1: Coronavirus Bond Simulation and Pricing

Step 1: Rolling Cases Simulation

Result: one pandemic spread path in days

for $j = 1, 2, \ldots$ *(in days)* **do**

Generate $R_0 \sim \Gamma(\text{shape}, \text{rate})$;

Obtain $R_c = \frac{\mathsf{E}(R_c)}{\mathsf{E}(R_0)} R_0$;

Generate $T_c \sim \exp(\text{mean}^{-1})$;

$\beta(j) = \gamma R_0$ if $j < T_c$ and $\beta = \gamma R_c$ if $j \geq T_c$;

Generate no. moving from S to I from time $j-1$ to $j \sim \text{Poisson}(\frac{\beta(j)S(j-1)I(j-1)}{N})$;

Generate no. moving from I to R from time $j-1$ to $j \sim \text{Binomial}(I(j-1), \gamma)$;

Update $S(j)$, $I(j)$ and $R(j)$ from $S(j-1)$, $I(j-1)$ and $R(j-1)$;

Obtain cumulative cases, $CC_t = N - S(j)$;

Obtain maximum rolling cases in period t:

$RC_1^{(p)} = \max_{s \in (p,1]} (CC_s - CC_{s-p})$ or $RC_t^{(p)} = \max_{s \in (t-1,t]} (CC_s - CC_{s-p})$ for $t = 2, 3, \ldots, n$

Event duration, T_E=no. of days until $I(j) = 0$;

end

Step 2: Frequency Simulation

Result: event starting dates within n years, $\mathfrak{T}^s = \{T_i^s\}_{i=1,2,\ldots}$

$T = 0$, $i = 1$, $\mathfrak{T}^s = \emptyset$;

while $T < n$ **do**

Generate $T_i \sim \exp(\text{mean}^{-1})$;

if $T + T_i \geq n$ **then**

end the loop;

else

Sample T_E^* from T_E (from Step 1);

$\mathfrak{T}^s = \mathfrak{T}^s \cup T_i^s$;

$T_i^s = T + T_i$;

$T = T + T_i + T_E^*$;

$i = i + 1$;

end

end

Step 3 Bond Pricing

Result: bond premium V

for *each year* t **do**

Calculate $\mathbb{P}$-measure probabilities $\mathsf{P}[RC_t^{(p)} < x]$ and $\mathsf{P}[RC_t^{(p)} < y]$;

Perform Wang transform on the two probabilities above to obtain $\mathsf{P}^{\mathbb{Q}}$;

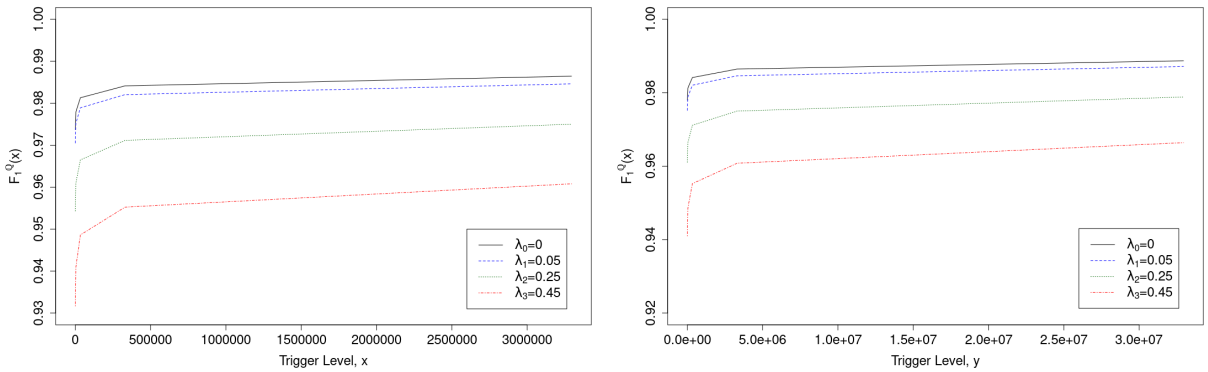
Calculate trigger probabilities under $\mathbb{Q}$: $1 - \mathsf{P}^{\mathbb{Q}}[RC_t^{(p)} < x]$ and $1 - \mathsf{P}^{\mathbb{Q}}[RC_t^{(p)} < y]$;

end

Calculate the coupon rate by solving, $V = \sum_{t=1}^{n} \mathsf{E}^{\mathbb{Q}}(\text{payout}_t) \times d(0,t) = f$.

principal value, f, to be \$1000 and the bond price to be \$1000, i.e., the bond will be sold at par. We will solve the maximum coupon rate, b/f. We set the trigger level as percentages of the entire U.S. population. Three sets of different trigger levels are presented: $x = 0.0001\%N, 0.01\%N, 1\%N$ and $y = 10x$. We also set $c_1 = x$ and $c_2 = y$.[15] Since the coronavirus bond is a hypothetical product with no market price observations, we assume different levels of market price of risk $\lambda \in \{\lambda_0, \lambda_1, \lambda_2, \lambda_3\} = \{0, 0.05, 0.25, 0.45\}$.[16] In addition, we assume the rolling window is two weeks.[17].

Figures 4a and 4b show the probabilities of not reaching the two triggers in the first year of the bond before and after the Wang transform. The $\lambda_0 = 0$ case corresponds to probabilities before the Wang transform, which can also be interpreted as pricing with zero market price of risk, i.e., the physical probability measure. The cases with $\lambda > 0$ correspond to probabilities after the Wang transform.



(a) Trigger Level x

(b) Trigger Level y

Figure 4: Probabilities below triggers. Figure 4a and Figure 4b display probabilities of not reaching triggers x and y, respectively. The case with $\lambda_0 = 0$ corresponds to probabilities before Wang transform while the cases with $\lambda > 0$ correspond to probabilities after Wang transform.

The probabilities of reaching different trigger levels each year under the physical probability

[15] We sensitivity test these parameters in Section 5.

[16] Because we do not have any observed market price for pandemic securities, we refer to the mortality-linked security market for a reasonable range of λ values. Lin and Cox (2005) estimate the market price of mortality risk to be 0.1792 for males and 0.2312 for females. Cairns et al. (2006) estimate the market price of longevity risk is 0.175. Lin and Cox (2007) determine that the market price of risk of annuity is 0.2134 and that of life insurance is 0.1933. Denuit et al. (2007) estimate the market price of longevity risk to be 0.4722883 for men and 0.2966378 for women.

[17] In contrast, the rolling window in World Bank PEF is 12 weeks. Many IDA countries were deprived of receiving the funds timely due to the long rolling window together with its complicated triggering mechanism.

measure (i.e., without Wang transform) are summarized in Table 3. In the t-th period, $\mathsf{P}[RC_t^{(p)} \geq x]$ (in both Designs BCFP and BCBP) and $\mathsf{P}[RC_t^{(p)} \geq y]$ (only in Design BCBP) represent the probabilities that the coupon reduction and the principal reduction are triggered, respectively. All probabilities shown in Table 3 are generally low, indicating acceptable risk from investors' viewpoint. We also observe that the probabilities during the first year are generally lower than those in the other two years. This is because we assume no ongoing pandemic event when the bond is first launched. Therefore, in Year 1, coupon and principal payouts can only be affected by pandemic events that start in the same year. In contrast, any pandemic event starting in the first or second year can still affect subsequent years. Thus, trigger probabilities during the first year are expected to be lower. In addition, higher values of x and y mean more stringent triggers and thus imply smaller trigger probabilities.

Table 3: Bond Trigger Probability in %

x/N (%)	0.0001			0.01			1		
y/N (%)	0.001			0.1			10		
Year	1	2	3	1	2	3	1	2	3
$\mathsf{P}[RC_t^{(p)} \geq x]$	2.63	4.70	4.94	1.87	3.22	3.32	1.36	2.14	2.20
$\mathsf{P}[RC_t^{(p)} \geq y]$	2.20	3.87	3.89	1.59	2.60	2.61	1.13	1.69	1.72

The pricing results are presented in Table 4. Panel A displays coupon rates of 3-year risk-free bonds that always pay full principal and full coupons. Panels B and C show the coronavirus bond's coupon rates with Design BCFP and BCBP, respectively. In general, coronavirus bonds have higher coupon rates than risk-free bonds, indicating that investors are compensated for bearing the pandemic risk. As expected, we observe that the coupon rate increases with an increasing market price of risk. An increasing trigger level leads to lower coupon rates because the probability of reaching the higher trigger decreases, reducing the risk of losing coupons or principal. Moreover, we also observe significant differences in rates between Design BCFP and Design BCBP. More risk-seeking investors may be interested in purchasing a variable principal (BCBP) structure. This indicates that the principal payout reduction structure has a more significant impact on coronavirus coupon rates than the market price of risk, as the principal payment accounts for a huge portion of the security value.

For illustration, Figure 5 plots coupon rates for Designs BCFP and BCBP. We see that coupon rates of BCFP are only slightly higher than that of a risk-free bond, whereas the coupon rates of BCBP are much higher. This is because a variable principal structure entails much higher risks, with both coupon and principal payouts dependent on pandemic

Table 4: Coronavirus Bond Coupon Rate Summary in %

Interest rate	1%			2%			3%		
x/N (%)	0.0001	0.01	1	0.0001	0.01	1	0.0001	0.01	1
y/N (%)	0.001	0.1	10	0.001	0.1	10	0.001	0.1	10
Panel A: Risk-Free Bond (RFB)									
	1.000	1.000	1.000	2.000	2.000	2.000	3.000	3.000	3.000
Panel B: Design Binary Coupon and Fixed Principal (BCFP)									
CB $\lambda_0 = 0$	1.043	1.029	1.019	2.085	2.058	2.039	3.127	3.086	3.058
CB $\lambda_1 = 0.05$	1.048	1.032	1.022	2.095	2.065	2.044	3.142	3.097	3.065
CB $\lambda_2 = 0.25$	1.073	1.051	1.035	2.145	2.101	2.070	3.217	3.151	3.105
CB $\lambda_3 = 0.45$	1.108	1.077	1.055	2.216	2.154	2.109	3.324	3.231	3.163
Panel C: Design Binary Coupon and Binary Principal (BCBP)									
CB $\lambda_0 = 0$	4.483	3.349	2.557	5.519	4.374	3.574	6.555	5.399	4.591
CB $\lambda_1 = 0.05$	4.902	3.649	2.767	5.943	4.677	3.787	6.983	5.705	4.806
CB $\lambda_2 = 0.25$	7.048	5.206	3.879	8.109	6.250	4.911	9.170	7.294	5.942
CB $\lambda_3 = 0.45$	10.132	7.496	5.554	11.224	8.563	6.603	12.316	9.630	7.652

Note: This table summarizes coupon rates for a 3-year coronavirus bond with face value \$1,000 sold at par. Panel A shows coupon rates of 3-year risk-free bonds that always pay full principal and full coupons, and the rest panels show coronavirus bond coupon rates with different design structures.

events. In contrast, a fixed principal structure is much safer for investors as a full principal payout is guaranteed. Investors have the flexibility to select different bond structures that satisfy their own levels of risk appetite. Figure 6 compares BCBP's coupon rates at different interest rates. A higher interest rate leads to higher coupon rates, as expected.

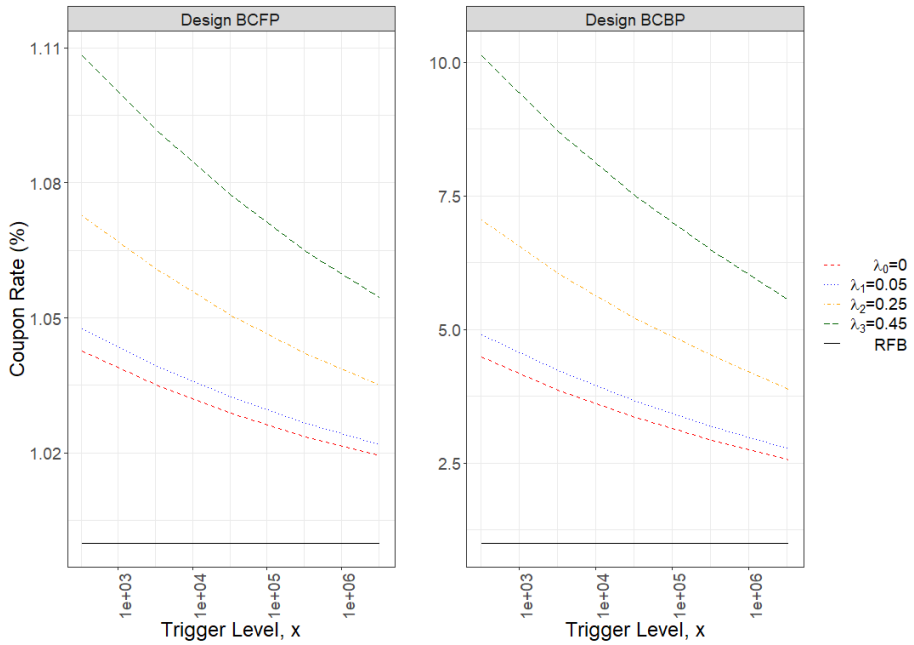


Figure 5: Coupon Rates of Different Designs (interest rate = 1%)

To analyze the investment returns for bond investors, we further calculate the average rate of return of the bond, r_{avg}. The average return, r_{avg}, is defined as

$$-V + \sum_{t=1}^{n} \frac{\mathsf{E}^{\mathbb{P}}[CIF_t]}{(1 + r_{\text{avg}})^t} = 0, \tag{8}$$

where $V = f$ is the coronavirus bond price (at par), and the expectation of cash inflows (CIF) is calculated under the physical probability measure. r_{avg} measures an investor's mean investment return. Table 5 summarizes r_{avg}. We observe that VP structures earn higher returns than FP structures due to their higher investment risk. In addition, the market price of risk parameter has a larger impact on VP designs. For example, under all interest rate assumptions, r_{avg} of BCFP is only up to 0.18% higher with $\lambda = 0.45$ than $\lambda = 0$. In contrast, for BCBP, the differences are all more than 2.8%.

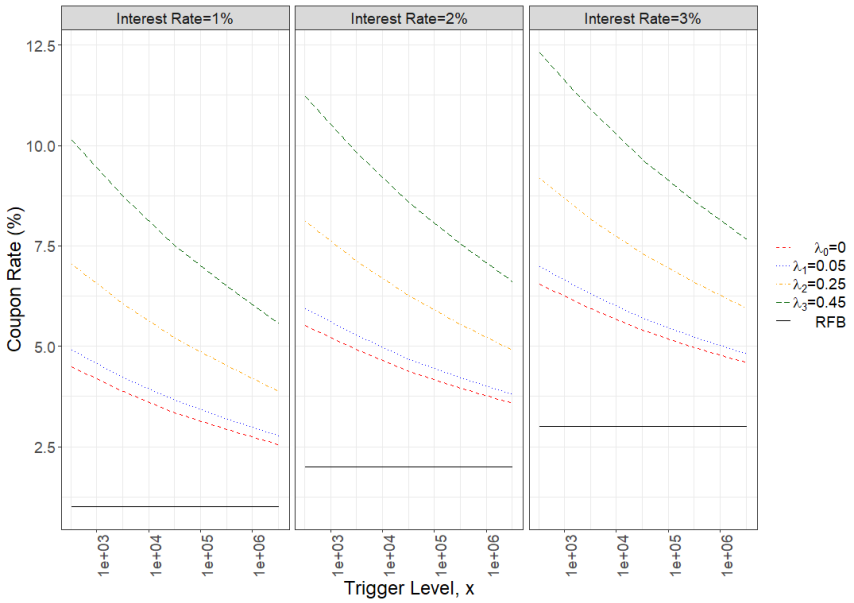


Figure 6: Coupon Rates Design BCBP at Different Interest Rates

Table 5: The Bond Average Return r_{avg} (in %) for a 3-year coronavirus bond with face value \$1,000 sold at par estimated based on Equation (8)

Interest rate		1%			2%			3%	
x/N (%)	0.0001	0.01	1	0.0001	0.01	1	0.0001	0.01	1
y/N (%)	0.001	0.1	10	0.001	0.1	10	0.001	0.1	10
Panel A: Risk-Free Bond (RFB)									
	1.000	1.000	1.000	2.000	2.000	2.000	3.000	3.000	3.000
Panel B: Design Binary Coupon and Fixed Principal (BCFP)									
CB $\lambda_0 = 0$	1.001	1.001	1.001	2.000	2.000	2.000	3.000	3.000	3.000
CB $\lambda_1 = 0.05$	1.006	1.004	1.003	2.009	2.007	2.005	3.014	3.010	3.007
CB $\lambda_2 = 0.25$	1.030	1.022	1.016	2.058	2.042	2.031	3.086	3.064	3.046
CB $\lambda_3 = 0.45$	1.064	1.048	1.036	2.126	2.094	2.069	3.189	3.141	3.104
Panel C: Design Binary Coupon and Binary Principal (BCBP)									
CB $\lambda_0 = 0$	1.001	1.001	1.001	2.000	2.000	2.000	3.000	3.000	3.000
CB $\lambda_1 = 0.05$	1.408	1.295	1.209	2.409	2.296	2.209	3.413	3.299	3.211
CB $\lambda_2 = 0.25$	3.476	2.812	2.300	4.501	3.831	3.314	5.525	4.849	4.328
CB $\lambda_3 = 0.45$	6.454	5.046	3.947	7.508	6.087	4.978	8.561	7.128	6.009

4.1.3 Coronavirus Bond Hedging Performance

We now investigate, from the government's perspective, the effectiveness of managing the pandemic risk using the proposed coronavirus bond. We conduct the analysis by assuming the following:

- The bond issuer is the U.S. government;
- The losses incurred from a coronavirus event are \$1 per infected case;
- Interest rate = inflation rate = 1%;
- Market price of risk is $\lambda = 0.45$.

We use 10,000 rounds of simulations for both rolling cases and frequency to calculate the optimal face value of the coronavirus bond, assuming only one of the bond designs, BCFP or BCBP, is issued, respectively. The optimal face value minimizes the 99% Value-at-Risk (VaR) of the net losses. Table 6 summarizes the optimal face values and the hedging effectivenesses of the two bond designs. Negative values indicate losses. Panel A shows the 99% VaR of losses from possible coronavirus events if the government does not issue any coronavirus bond. Panels B and C show the 99% VaR of the net losses from the bond and coronavirus events if the optimal face value of BCFP or BCBP is issued to hedge the coronavirus risk, respectively. Design BCFP is expected to have a higher optimal face value because its fixed principal design is less compensating from the issuer's perspective than design BCBP in case of coronavirus events. Only the coupon payouts of design BCFP can be retained during severe coronavirus events, whereas both the coupon and principal payouts of design BCBP can be retained. Thus, a much higher quantity of BCFP is required to achieve similar hedging effects of BCBP. Therefore, while the 99% VaR reduction is around 80% for both designs, we observe a much higher optimal face value of design BCFP compared to design BCBP – the former is about 100 times the latter. Although both designs can be useful in pandemic risk management, it might not be practical to sell as much fixed principal bond alone. Moreover, we observe that the optimal face value increases with trigger levels for both designs. This is expected following similar arguments that higher trigger levels imply lower per-unit protection for the issuer, requiring a higher quantity to achieve similar hedging effects.

We further assume that the government wishes to issue two tranches of the bond – Class A and Class B – with a fixed total face value of \$500 million. Class A has a BCFP design, and Class B has a BCBP design, entailing different levels of risk. We calculate the optimal proportion of the two classes to minimize the 99% VaR of the net losses. Panel D of Table 6 shows the optimal proportion of Class A bond (BCFP). We observe that with a total face value of \$500 million, the optimal quantity of the Class B bond is slightly higher than that of the Class A bond. As the trigger level increases, both BCFP and BCBP designs have lower protections, requiring relatively more class (Class B) to achieve a similar hedging

effect. Therefore, the proportion of the Class B bond increases with trigger levels. The 99% VaR reductions are similar to those with only bond BCBP issued. These results give the government insights into the amount of coronavirus bond to issue to optimally hedge the coronavirus risk.

Table 6: The impact of hedging the pandemic risk with Design BCFP and BCBP

$x/N(\%)$	0.0001	0.01	1
$x/N(\%)$	0.001	0.1	10
Panel A: No Bond			
99% VaR of Loss ($million)		-324.47	
Panel B: Bond Design BCFP			
Face Value ($million)	28,387.85	29,515.71	30,848.43
99% VaR of Net Losses ($million)	-93.15	-69.17	-51.59
99% VaR Reduction (%)	71.29	78.68	84.10
Panel C: Bond Design BCBP			
Face Value ($million)	272.87	285.51	310.18
99% VaR of Net Losses ($million)	-75.52	-56.35	-44.86
99% VaR Reduction (%)	76.76	82.63	86.17
Panel D: Mixture of BCFP and BCBP (Total Face Value of $500 million)			
Class A (BCFP) Proportion (%)	45.97	43.36	38.38
99% VaR of Net Losses ($million)	-75.52	-56.39	-44.81
99% VaR Reduction (%)	76.72	82.62	86.19

4.1.4 Backtesting the COVID-19

This section further assesses the viability of the proposed coronavirus bond in hedging the pandemic risk, by backtesting the ongoing COVID-19 pandemic (Johns Hopkins, 2022). Suppose the U.S. government issued a coronavirus bond on Jan 1, 2019, for a term to maturity of 3 years with a total face value of $500 million. There are two tranches issued – Class A with a BCFP design and Class B with a BCBP design. All other assumptions are the same as in Section 4.1.3 and the optimal proportions of the two classes are issued.

The first confirmed COVID-19 case in the U.S. was reported on Jan 22, 2020. The coupon and principal payouts in the second and third periods (2020 and 2021) are then reduced based on the assumed trigger levels accordingly. Gains or losses from the coronavirus bond are presented in Table 7. Losses from COVID-19 are proportional to the number of confirmed cases by the bond maturity date ($1 per case). Gains or losses from each class

are compounded to the bond maturity date (Dec 31, 2021). Positive values indicate net gains, while negative values indicate net losses from the bond. The total gains or losses are obtained by summing up the gains or losses from COVID-19 cases and the two classes of bond. We can see that the coronavirus bond yields a total gain for the first two trigger level sets ($x/N = 0.0001\%$ and 0.01%). In these cases, the reduction in the coronavirus bond payouts can be used by the government to fund the rising medical expenditure due to COVID-19 and additional medical infrastructure to prepare for future pandemic events. For the highest trigger level set ($x/N = 1\%$ and $y/N = 10\%$), the total loss is higher than the loss from COVID-19 because the second trigger level y is not met, and thus, the principal payout in Class B bond is still paid to investors. Although this bond specification does not help reduce the total loss from COVID-19, it can still be useful in the case of more severe coronavirus events, as indicated in our previous analysis shown in Table 6. Moreover, we observe that the magnitudes of gains or losses from Class B bond (BCBP) are much larger than those from Class A bond (BCFP) even though the total face value of Class A bond is similar to that of Class B bond. This is expected because the Class B bond provides higher per-unit protection with a possible reduction in the principal amount, leading to much higher variability in its cash flows than the Class A bond with the same face value issued.

Table 7: Gains/Losses from the Coronavirus Bond in $millon

$x/N(\%)$	0.0001	0.01	1
$y/N(\%)$	0.001	0.1	10
Loss from COVID-19	-54.84	-54.84	-54.84
Gain/Loss from Class A Bond (BCFP)	4.37	4.19	1.71
Gain/Loss from Class B Bond (BCBP)	250.42	270.12	-25.40
Total Gain/Loss	199.95	219.47	-78.53

4.2 Dengue Swap

4.2.1 Dengue Simulation Model

Dengue is an endemic that creates important public health concerns in tropical and subtropical climate areas. In this subsection, we discuss a dengue swap as an example of the endemic swap design. For dengue simulation, we employ a widely used SIR-SEI transmission model that considers seasonal variations in the vector population (i.e., the population of mosquitoes) (Andraud et al., 2013; Burattini et al., 2008; Coutinho et al., 2005; 2006). Figure 7 shows the transmission process represented by the SIR-SEI model. This model is proposed by Andraud et al. (2013) and is applied to dengue cases in Singapore.

In several ways, this dengue epidemiological model is different from the pandemic model

in Subsection 4.1. First, two populations are involved in the system – the host population (denoted by the index h) and the vector population (denoted by the index v). Instead of human-to-human or vector-to-vector transmission, dengue transmission occurs between humans and vectors through mosquito bites. Thus, the susceptible host (i.e. human) population, $S_h(t)$, interacts with the infectious vector population, $I_v(t)$, and the infectious human population, $I_h(t)$, interacts with the susceptible vector population, $S_v(t)$, to transmit dengue disease. Second, an endemic like the dengue virus has a persistent presence in the human population for a long time (longer than 10 years) (see, e.g., Ooi et al., 2006; Rajarethinam et al., 2018). Therefore, the changes to both the host population and the vector population need to be taken into account. Hence for the respective host and vector populations, the recruitment rates, $H(t)$ and $A(t)$, and the death rates, μ_h and μ_v, are included to account for the changes in the host and vector population. As a result, the total human population, $N_h(t) = S_h(t) + I_h(t) + R_h(t)$, is time-varying. Finally, the transition of the status of the vectors is also different from that of the human population. More specifically, upon infection, the susceptible vectors, $S_v(t)$, first move to an incubation stage, $E_v(t)$, before they become infectious in $I_v(t)$.

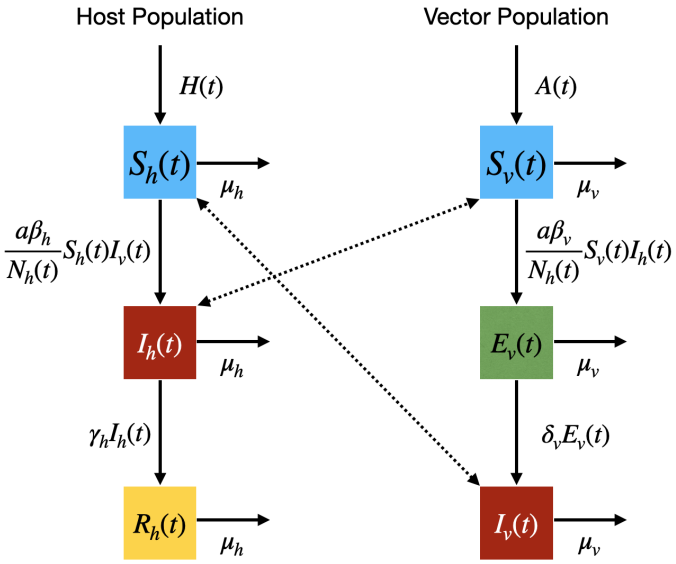


Figure 7: Dengue SIR-SEI Model. Solid arrows represent transitions of status within the same population, and dotted arrows represent interactions between the host and the vector population.

The deterministic transmission process is governed by a set of ODEs in Equation (9) for

the host population and Equation (10) for the vector population:

$$\begin{aligned}
\frac{dS_h(t)}{dt} &= H(t) - \frac{\beta_h a}{N_h(t)} S_h(t) I_v(t) - \mu_h S_h(t), \\
\frac{dI_h(t)}{dt} &= \frac{\beta_h a}{N_h(t)} S_h(t) I_v(t) - (\gamma_h + \mu_h) I_h(t), \\
\frac{dR_h(t)}{dt} &= \gamma_h I_h(t) - \mu_h R_h(t),
\end{aligned} \tag{9}$$

and

$$\begin{aligned}
\frac{dS_v(t)}{dt} &= A(t) - \frac{\beta_v a}{N_h(t)} S_v(t) I_h(t) - \mu_v S_v(t), \\
\frac{dE_v(t)}{dt} &= \frac{\beta_v a}{N_h(t)} S_v(t) I_h(t) - (\delta_v + \mu_v) E_v(t), \\
\frac{dI_v(t)}{dt} &= \delta_v E_v(t) - \mu_v I_v(t).
\end{aligned} \tag{10}$$

Recall that the recruitment numbers $H(t)$ and $A(t)$ and the death rates μ_h and μ_v are for the respective host and vector populations. By defining μ_g as the host recruitment rate, the host population size at time t and the host recruitment number $H(t)$ are related via $H(t) = \mu_g N_h(t)$. μ_h and μ_v are the death rates of the human population and vector population, respectively. Furthermore, β_h and β_v are the probabilities of transmission from vector to host and host to vector, respectively; a is the biting rate, which is calculated as the average number of blood meals taken by a female vector; the vector population recruitment rate $A(t)$ reflects the seasonality of the vector population through a cosine function given by

$$A(t) = A_0(t)(1 + \epsilon \cos(\omega t + \psi)), \tag{11}$$

where $\omega = \frac{2\pi}{365}$ corresponds to a one-year period, ϵ represents the amplitude of seasonal variations, and $A_0(t)$ is the average vector recruitment at time t. Andraud et al. (2013) assume $A_0(t)$ to be constant over time. In our analysis, we allow $A_0(t)$ to be linearly time-varying:

$$A_0(t) = A_0 + mt, \tag{12}$$

where m is the increment rate and A_0 is a constant.

While the human population data, including population size, $N_h(t)$, birth rate, μ_g, and death rate, μ_h, can be readily obtained from census data, there is usually a lack of data on the vector population, especially the size of infectious vectors and the growth rate of vectors. In particular, the initial average vector recruitment rate, A_0, increment rate of $A_0(t)$, m, and the initial number of infectious vectors, $I_v(0)$, are key parameters in this model that determine the number of dengue infections but are unavailable in the existing

literature. Therefore, we estimate the values of A_0, m, and $I_v(t)$ by fitting the model based on Equations (9)-(12) using weekly dengue cases in Singapore from 2014 to 2020 (MOH Singapore, 2019; NEA Singapore, 2020) by minimizing the sum of squared errors. The host recruitment rate, μ_g, is approximated as the average growth rate. The host death rate, μ_h, is approximated using the crude death rate in Singapore. Details of all parameter definitions and initial values are summarized in Table 8.

In the simulation, we calculate a deterministic path from 2014 to 2020 with the previously fitted model (i.e., Equations (9)-(12)) using Euler's method with a step size of 1 day. All parameter values are summarized in Table 8 and are either assumed from literature or estimated. The values $N_h(t)$, $S_h(t)$, $I_h(t)$, $R_h(t)$, $S_v(t)$, $E_v(t)$, $I_v(t)$ at the end of 2020 evaluated from the deterministic path are then used as the initial values for a stochastic simulation from 2021. The stochastic model follows the ODEs in Equations (9) and (10) and follows similar assumptions in the stochastic pandemic SIR model discussed in Subsection 4.1. In particular, the number of hosts moving from state S_h to state I_h and the number of vectors moving from state S_v to state E_v are Poisson random variables. The number of hosts moving from state I_h to state R_h and the number of vectors moving from state E_v to state I_v are Binomial random variables. Step 1 of Algorithm 2 describes details of the dengue simulation process. 10,000 simulation paths are generated.

4.2.2 Dengue Swap Pricing Results

We price an n-year Dengue Swap which matures at the end of year n ($n = 1, \ldots, 8$) and exchanges floating and fixed payments semi-annually. The pricing process of the dengue swap is described by Step 2 of Algorithm 2. Figure 8 displays the empirical CDF of simulated dengue cases in the first half of 2021, with different values of the market price of risk, $\lambda = \{\lambda_0, \lambda_1, \lambda_2, \lambda_3\} = \{0, 0.05, 0.25, 0.45\}$. The pricing results are presented in Table 9. As expected, higher market prices of risk lead to higher fixed payments. The difference between fixed payments evaluated at different interest rates is small. In addition, since the floating payments are not monotonically changing over the years, the fixed payments may increase or decrease with an increasing interest rate with a given term to maturity.

To see how the proposed dengue swap can serve as an effective risk mitigation tool from the hedger's point of view, we consider a dengue insurer that is liable to pay \$1 per dengue case that occurred in Singapore. We calculate the annual payments of the hedger before and after purchasing dengue swaps and summarize the results in Table 10. Panel A shows quantiles of annual payments for dengue claims without dengue swaps. Panel B shows fixed annual payments (i.e., twice semiannual payments) after hedging with dengue swaps. We can see that dengue swaps can effectively stabilize hedger's cash flows. Therefore, insurers may use the swap as an effective and flexible instrument to manage their risk exposure to endemic policies.

Table 8: Dengue SIR-SEI Model Parameters

Parameter	**Definition**	**Value**	**Reference**
$H(t)$	Host recuritment number	$\mu_g N_h(t)$	Calculated
μ_g (years^{-1})	Host recruitment rate	1.4194%	IBRD (2020)
μ_h (years^{-1})	Host death rate	0.5%	MOH Singapore (2020)
μ_v^{-1} (days)	Vector life expectancy	14.49	Fouque et al. (2006)
γ_h^{-1} (days)	Infectious period	6	Halstead (2007)
δ_v^{-1} (days)	Extrinsic incubation period	10	Rigau-Pérez et al. (1998)
b (days^{-1})	Biting rate	0.76	Scott et al. (2000)
β_h	Probability of transmission from vector to host	0.75	Newton and Reiter (1992)
β_v	Probability of transmission from host to vector	0.75	Newton and Reiter (1992)
T_0	Initial time for simulation	Start of 2014	Start of data sample
$N_h(0)$	Total Singaporean population at the end of 2013	5,399,162	IBRD (2020)
$S_h(0)$	Initial proportion of susceptible individuals at T_0(%)	56.9	Ooi et al. (2001)
$I_h(0)$	Dengue cases in the 1st week of 2014 (an approximate of the initial no. of infectious hosts	437	MOH Singapore (2019)
$E_v(0)$	Initial no. of exposed vectors	0	Andraud et al. (2013)
ϵ	Factor of periodic forcing	0.22	Andraud et al. (2013)
ψ	Phase of periodic forcing	-2.93	Andraud et al. (2013)
A_0	Initial average recruitment rate	39.445	Estimated
m	Increment rate of $A_0(t)$	0.5845	Estimated
$I_v(0)$	Initial no. of infectious vectors	391	Estimated

Algorithm 2: Dengue Swap Simulation and Pricing

Step 1 Dengue Case Simulation

Result: one dengue spread path in days

for $t = 1, 2, \ldots$ *(in days)* **do**

Generate no. moving from S_h to I_h from time $t-1$ to $t \sim \text{Poisson}(\frac{a\beta S_h(t-1) I_v(t-1)}{N_h(t-1)})$;

Generate no. moving from I_h to R_h from time $t-1$ to $t \sim \text{Binomial}(I_h(t-1), \gamma_h)$;

Generate no. moving from S_v to E_v from time $t-1$ to $t \sim \text{Poisson}(\frac{a\beta S_v(t-1) I_h(t-1)}{N_h(t-1)})$;

Generate no. moving from E_v to I_v from time $t-1$ to $t \sim \text{Binomial}(E_v(t-1), \gamma_v)$;

Calculate the change in numbers in each state from $t-1$ to t;

Update $S_h(t)$, $I_h(t)$, $R_h(t)$, $S_v(t)$, $E_v(t)$, and $I_v(t)$ from $S_h(t-1)$, $I_h(t-1)$, $R_h(t-1)$, $S_v(t-1)$, $E_v(t-1)$, and $I_v(t-1)$;

Daily dengue cases, $x(t)$ =no. moving from S_h to I_h from time $t-1$ to t;

end

Step 2 Swap Pricing

Result: aggregated semi-annual cases

for *each half-year* **do**

Aggregate daily cases, $x(t)$;

Obtain the empirical CDF of semi-annual cases;

Perform Wang transform;

Calculate expected no. of cases after Wang transform;

end

Calculate fixed payment based on the expected no. of cases after Wang transform.

5 Sensitivity Analysis

5.1 The Effect of Reinfection

Recent studies have shown that COVID-19 mutations such as Delta and Omicron can escape immunity and lead to reinfections (Eggink et al., 2021; Karim and Karim, 2021; Townsend et al., 2021). The SIR model presented in Subsection 4.1 can be modified to include possible loss of natural immunity from infection, as shown in Figure 9. The "removed" individuals, $R(t)$, are now classified as either $R_D(t)$ (dead) or $R_A(t)$ (recovered) with a coronavirus fatality rate of α. Of those recovered patients, a fraction of η transit back to the "susceptible" state. The model resembles the formulation in Zhai et al. (2021) and Malkov (2020).

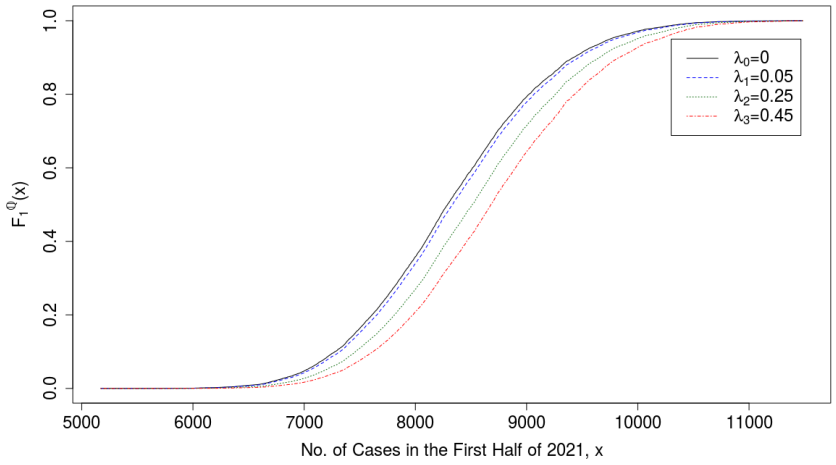


Figure 8: Dengue Cases CDF before and after Wang Transform. The case with $\lambda_0 = 0$ corresponds to probabilities before Wang transform while the cases with $\lambda > 0$ correspond to probabilities after Wang transform.

Table 9: Summary of Dengue Swap Fixed Payments

Term to Maturity	1	2	3	4	5	6	7	8
Panel A: Interest rate = 1%								
$\lambda_0 = 0$	11,755	11,634	11,434	11,193	10,930	10,657	10,384	10,123
$\lambda_1 = 0.05$	11,849	11,756	11,574	11,343	11,087	10,819	10,549	10,291
$\lambda_2 = 0.25$	12,230	12,253	12,141	11,953	11,724	11,474	11,218	10,972
$\lambda_3 = 0.45$	12,618	12,758	12,721	12,577	12,375	12,144	11,903	11,669
Panel B: Interest rate = 2%								
$\lambda_0 = 0$	11,746	11,626	11,429	11,191	10,932	10,664	10,398	10,144
$\lambda_1 = 0.05$	11,840	11,748	11,568	11,340	11,088	10,826	10,562	10,311
$\lambda_2 = 0.25$	12,221	12,244	12,134	11,948	11,723	11,479	11,229	10,989
$\lambda_3 = 0.45$	12,608	12,748	12,711	12,570	12,371	12,146	11,910	11,683
Panel C: Interest rate = 3%								
$\lambda_0 = 0$	11,738	11,618	11,423	11,188	10,933	10,672	10,412	10,164
$\lambda_1 = 0.05$	11,832	11,740	11,562	11,337	11,089	10,832	10,575	10,331
$\lambda_2 = 0.25$	12,212	12,235	12,126	11,943	11,722	11,483	11,239	11,006
$\lambda_3 = 0.45$	12,598	12,738	12,702	12,562	12,368	12,148	11,918	11,697

Table 10: The Effectiveness of Dengue Swaps for Hedging Endemic Risk

Panel A: Quantiles of Annual Payments for Dengue Claims								
Year	1	2	3	4	5	6	7	8
5th Quantile	17,829	13,868	11,512	9,538	8,321	7,130	6,188	5,267
10th Quantile	19,002	15,600	13,525	11,903	10,587	9,399	8,438	7,198
25th Quantile	20,987	18,824	17,146	15,843	14,668	13,388	12,194	11,137
50th Quantile	23,340	22,754	21,691	20,584	19,337	18,054	16,860	15,898
75th Quantile	25,888	26,848	26,447	25,513	24,469	23,327	22,073	21,183
90th Quantile	28,267	30,863	31,050	30,293	29,308	28,054	27,045	26,393
95th Quantile	29,898	33,295	34,170	33,351	32,341	31,245	30,273	29,573
Panel B: Fixed Annual Payments from Dengue Swaps								
Term to Maturity	1	2	3	4	5	6	7	8
$\lambda_0 = 0$	23,509	23,268	22,869	22,386	21,859	21,314	20,769	20,247
$\lambda_1 = 0.05$	23,698	23,513	23,148	22,687	22,173	21,637	21,098	20,582
$\lambda_2 = 0.25$	24,460	24,506	24,283	23,907	23,448	22,949	22,437	21,944
$\lambda_3 = 0.45$	25,235	25,517	25,441	25,153	24,749	24,288	23,805	23,338

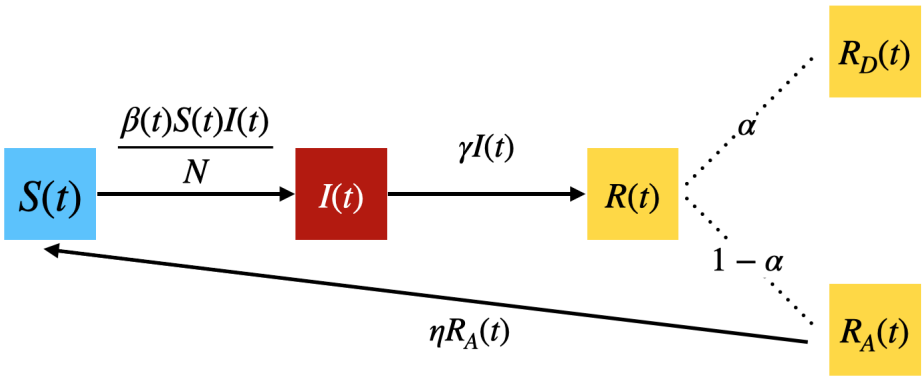


Figure 9: Pandemic SIR model with Possible Loss of Immunity

Equation (7) can be modified as follows:

$$\begin{aligned}
\frac{dS(t)}{dt} &= -\frac{\beta(t)S(t)I(t)}{N} + \eta(1-\alpha)R(t), \\
\frac{dI(t)}{dt} &= \frac{\beta(t)S(t)I(t)}{N} - \gamma I(t), \\
\frac{dR(t)}{dt} &= \gamma I(t) - \eta(1-\alpha)R(t),
\end{aligned} \tag{13}$$

where η is the immunity loss rate, and α is the fatality rate of coronavirus. We set $\alpha = 0.75\%$, which is re-estimated based on the historical fatality rates of coronavirus (IBRD, 2017b), by including the new data of the current COVID-19 pandemic (Johns Hopkins CRC, 2022). However, there is a lack of real data to estimate the immunity loss rate, η empirically. Zhai et al. (2021) assume a 1% immunity loss, and Malkov (2020) uses a range of different immunity loss rates in the simulations. We test the model with three different values: $\eta \in \{0, 0.01, 0.02\}$, which are within the range of immunity loss rates used by Zhai et al. (2021) and Malkov (2020). $\eta = 0$ corresponds to the baseline case in Subsection 4.1 where reinfection is impossible. The number of individuals moving from $R(t)$ to $S(t)$ is assumed to follow a Binomial distribution with an expectation of $\eta R_A(t)$.

Figure 10 shows the coupon rates of the BCBP structure with different immunity loss rates. Simulation models with higher immunity loss rates have higher coupon rates as expected since the probability of reaching the triggers is higher with the possibility of reinfections. At $\lambda_3 = 0.45$, the coupons rates for the BCBP structure at the lowest trigger levels are 10.132%, 11.152%, and 11.552% for $\eta = 0, 0.01, 0.02$ respectively. While an immunity loss rate of 0.01 raises the coupon rate by about 1% from the model with no loss of immunity, a double immunity loss rate of 0.02 only gives rise to a marginal increase in coupon rates.

5.2 Vaccination and Antiviral Controls

The SIR model in Subsection 4.1 assumes no vaccination or antiviral controls after the outbreak of coronavirus events. While vaccines and antiviral treatments were not available in any previous coronavirus event, COVID-19 vaccines and antiviral medications have been developed at an unprecedented speed. For example, the Pfizer-BioNTech COVID-19 Vaccine has been available under Emergency Use Authorization (EUA) since December 11, 2020. Pfizer's Paxlovid, the first oral COVID-19 antiviral treatment, was approved under EUA on December 22, 2021. Thus, in this subsection, we discuss the effects of vaccination and antiviral controls. We modify the SIR model following the formulation in De la Sen and Ibeas (2021). The corresponding ODEs are expressed in Equation (14), and the transition diagram is illustrated in Figure 11.

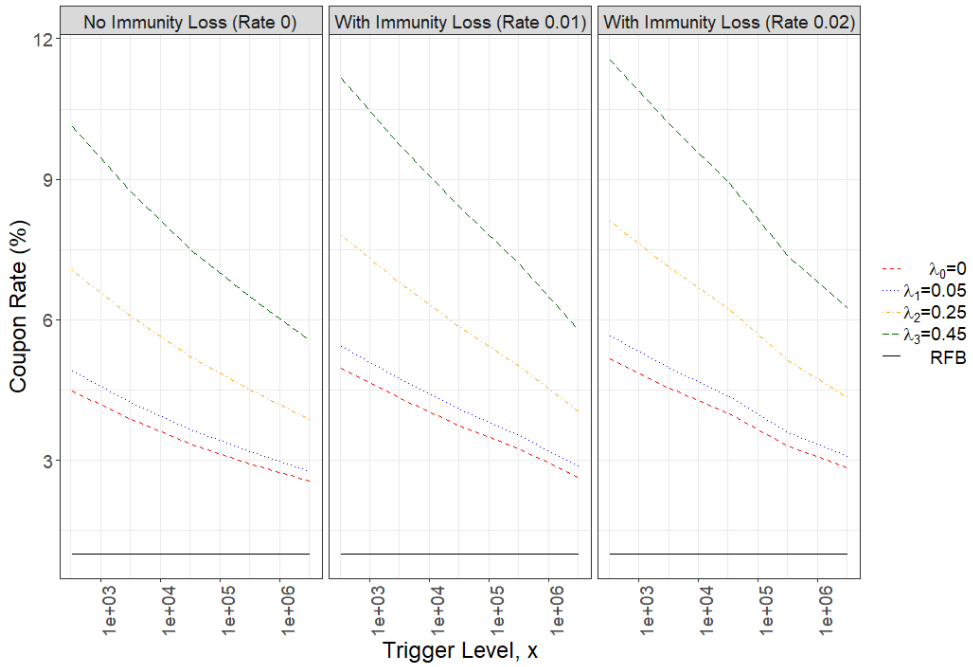


Figure 10: Coupon Rates of BCBP Structure with Loss of Immunity (interest rate = 1%)

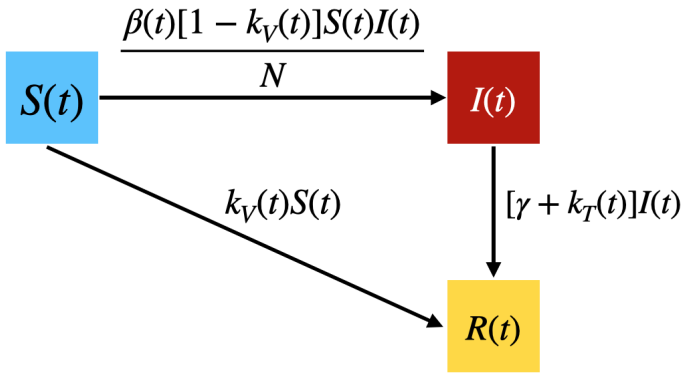


Figure 11: Pandemic SIR model with Vaccination and Antiviral Controls

$$
\begin{aligned}
\frac{dS(t)}{dt} &= -\frac{\beta(t)[1-k_V(t)]S(t)I(t)}{N} - k_V(t)S(t), \\
\frac{dI(t)}{dt} &= \frac{\beta(t)[1-k_V(t)]S(t)I(t)}{N} - [\gamma + k_T(t)]I(t), \\
\frac{dR(t)}{dt} &= [\gamma + k_T(t)]I(t) + k_V(t)S(t),
\end{aligned} \tag{14}
$$

where $k_V(t)$ is the daily vaccination rate of susceptible individuals ($k_V(t) = 0$ means no vaccination), and $k_T(t)$ is the improved recovery rate with antiviral treatment for infected patients, such that the number of individuals moving form $I(t)$ to $R(t)$ now follows a Binomial distribution with probability $\gamma + k_T(t)$ (as compared to a constant γ in Algorithm 1).

Following De la Sen and Ibeas (2021), we set $k_T(t) = 0$ before the launch of antiviral treatment and $k_T(t) = 0.004$ after that. Similarly, before the launch of vaccination $k_V(t) = 0$. We compare two values of $k_V(t)$ after the launch of vaccination. The first value is $k_V(t) = 0.001$, according to De la Sen and Ibeas (2021), and the second value is $k_V(t) = 0.0035$, according to the average daily vaccination rate in the U.S. from December 11, 2020 to December 29, 2021. The vaccine and antiviral treatment development time for COVID-19 is unprecedentedly fast with about one year after the initial outbreak. Therefore, we assume that one year is the minimum time required for vaccine development. The time to implement vaccination is then predicted by a distribution of $\text{Exp}(1/365) + 365$ days, and the time to implement antiviral treatment is assumed to be $\text{Exp}(1/365) + 600$ days.

Figure 12 shows the coupon rates of the BCBP structure with or without vaccines and antiviral treatment. The left-most graph shows coupon rates without any vaccines (Vac) or antiviral treatment (AT), i.e., $k_V(t) = k_T(t) = 0$ throughout. The middle graph shows coupon rates for $k_V(t) = 0.0010$ and $k_T(t) = 0.0040$ and the right-most graph shows coupon rates for $k_V(t) = 0.0035$ and $k_T(t) = 0.0040$ after vaccines and antiviral treatment become available. Comparing the middle and left-most graphs, we observe that simulation models with vaccines and antiviral treatments have lower coupon rates. Comparing the right-most and middle graphs, we observe that higher vaccination rates have lower coupon rates. These results make sense since the probabilities of reaching the triggers are lower with fewer possible infections due to vaccinations and a shorter period in the infectious state. We also observe that the impact of vaccination and antiviral treatment on coupon rates is small. For example, at $\lambda_3 = 0.45$, the coupons rates for the BCBP structure at the lowest trigger levels are 10.132%, 9.924%, and 9.740% for vaccination rates of $k_V(t) \in \{0, 0.0010, 0.0035\}$ and antiviral treatment rates of $k_T(t) \in \{0, 0.0040, 0.0040\}$, respectively. The unsizable reduction in coupon rates is due to the long development period of vaccines and antiviral treatments. Government interventions discussed in Subsection 4.1, including mask-wearing and social distancing policies, are likely to have curbed the spread of the virus effectively before vaccines are available. Moreover, since the bond's term to maturity is only three years, the bond is likely to have matured before vaccines, and antiviral controls

are approved.

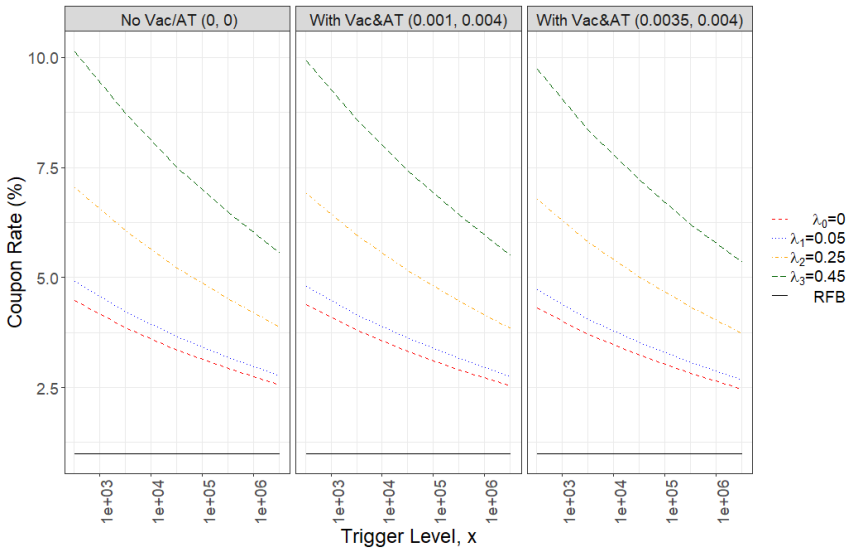


Figure 12: Coupon Rates of BCBP Structure with or without Vaccines and Antiviral Treatment (interest rate = 1%). The first graph on the left shows coupon rates without vaccines (Vac) or antiviral treatment (AT). The two graphs on the right show coupon rates with both vaccines and antiviral treatment. The two values in the brackets are the assumed vaccination rate and the antiviral treatment rate, respectively.

5.3 Other Parameters

In Subsection 4.1.1, we simulate and price coronavirus bond following IBRD's assumptions that pandemic event frequency follows an exponential distribution with mean of 15 years (Exp(1/15)) and the reproduction rate before containment follows a Gamma distribution ($R_0 \sim \Gamma(7.076, 2.505)$). In addition, in the double trigger bond structures (i.e., Designs VP), we set $y = 10x$. In this section, we sensitivity test these parameters.

Figure 13 shows prices of the BCBP bond structure with frequency increased to every 10 years or reduced to every 20 years at an interest rate of 1%. A higher frequency of pandemic events leads to higher coupon rates because of higher risks of losing coupons or principal; hence, investors earn higher investment returns. Figure 14 plots BCBP coupon rates with different R_0 distributions at an interest rate of 1%. With a higher reproduction rate, a pandemic spreads faster. Thus, the coupon rates increase due to higher trigger probabilities. We observe similar patterns to all other pandemic bond design structures.

Figure 15 shows the pricing results with $y = 5x$ and $y = 15x$ for the BCBP bond structure at an interest rate of 1%. We see that coupon rates only decrease slightly with an increasing

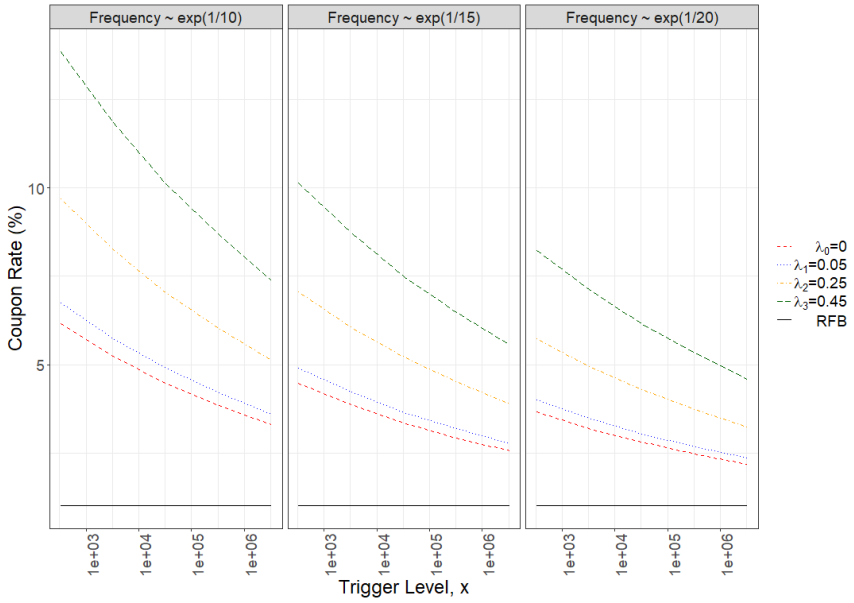


Figure 13: Coupon Rates of BCBP Structure with Different Frequency Distributions (interest rate = 1%)

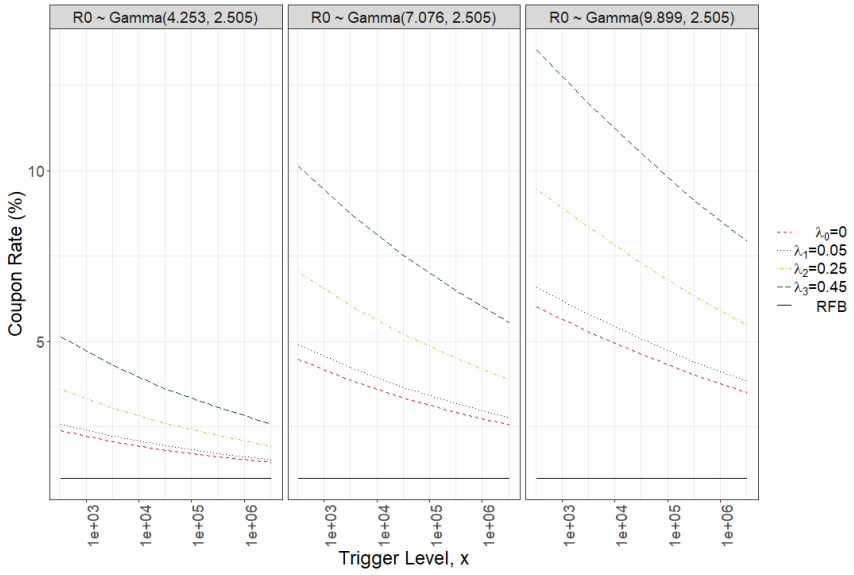


Figure 14: Coupon Rates of BCBP Structure with Different R_0 Distributions (interest rate = 1%)

ratio of the second trigger level, y, to the first trigger level, x. This indicates that coupon rates are not sensitive to the y/x ratio.

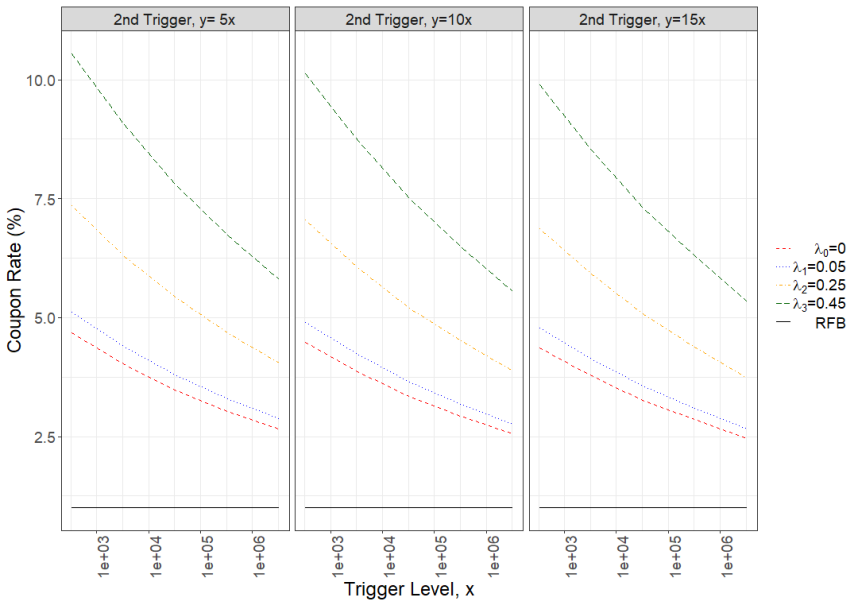


Figure 15: Coupon Rates of BCBP Structure with Different y/x Ratio (interest rate = 1%)

6 Discussion and Conclusion

While many financial innovations have been developed in the capital market to create new securities and risk management tools, including catastrophe bonds, mortality-linked securities, etc., pandemic bonds are still very new in the market. In 2017, the World Bank launched a first-ever pandemic bond. The PEF has been criticized for its complicated mechanism and overly stringent fund releasing criteria.

In this paper, we focus on developing securities that have the advantage of responding to epidemic events quickly and providing adequate capital for recovery plans. We propose two epidemic financing facilities: pandemic bonds and endemic swaps. Pandemic bonds are designed with simple structures and are responsive to provide timely capital in a severe pandemic outbreak. Endemic swaps can hedge a series of risky payments contingent on ongoing diseases within a geographic region. Using coronavirus as an example of pandemic and dengue fever as an example of endemic, we discuss the modeling and pricing of the proposed epidemic securities. Our empirical results show that the proposed securities can provide additional capital for pandemic recovery plans, effectively stabilize hedgers' cash flows, and create attractive returns for different investors.

This paper mainly focuses on the technical and actuarial aspects of designing epidemic facilities. We normalize the severity of losses to be \$1 per epidemic event. This way, all the monetary numbers analyzed in this paper are scalable. However, the severity of the loss is critical to the design of epidemic risk solutions. The modeling of loss severity is complicated as it depends on many factors such as the specific type of disease, economic development, medical expenses, etc. We may also need to model the dependence between the loss severity and epidemic frequency. In addition, in this paper, we discuss pandemic bond and endemic swaps separately. However, there may be some correlations between different epidemics. In that respect, an epidemic bond structure with multiple epidemics could offer a more effective hedging of epidemic risks. Such multi-epidemic securities may also be attractive to investors with various risk appetites. We leave these interesting issues for future research.

References

Allen, L. J. (2017). A primer on stochastic epidemic models: Formulation, numerical simulation, and analysis. *Infectious Disease Modelling 2*(2), 128–142.

Andraud, M., N. Hens, and P. Beutels (2013). A simple periodic-forced model for dengue fitted to incidence data in Singapore. *Mathematical Biosciences 244*(1), 22–28.

Barrieu, P. and L. Albertini (2010). *The handbook of insurance-linked securities*. John Wiley & Sons.

Baud, D., X. Qi, K. Nielsen-Saines, D. Musso, L. Pomar, and G. Favre (2020). Real estimates of mortality following COVID-19 infection. *The Lancet Infectious Diseases 20*(7), 773.

Bhapkar, H. R., P. N. Mahalle, N. Dey, and K. C. Santosh (2020). Revisited covid-19 mortality and recovery rates: Are we missing recovery time period? *Journal of Medical Systems 44*(12).

Blake, D., A. Cairns, G. Coughlan, K. Dowd, and R. MacMinn (2013). The new life market. *Journal of Risk and Insurance 80*(3), 501–558.

Blake, D. and A. J. Cairns (2020). Longevity risk and capital markets: The 2018–19 update. *Annals of Actuarial Science 14*(2), 219–261.

Bloom, D. E., C. Daniel, and J. Sevilla (2018). Epidemics and economics: New and resurgent infectious diseases can have far-reaching economic repercussions. *Finance and Development 55*(2), 46–49.

Braun, A. (2016). Pricing in the primary market for cat bonds: New empirical evidence. *Journal of Risk and Insurance 83*(4), 811–847.

Brockett, P. L., L. L. Goldens, M.-M. Wen, and C. C. Yang (2009). Pricing weather derivatives using the indifference pricing approach. *North American Actuarial Journal 13*(3), 303–315.

Brockett, P. L., M. Wang, and C. Yang (2005). Weather derivatives and weather risk management. *Risk Management and Insurance Review 8*(1), 127–140.

Burattini, M. N., M. Chen, A. Chow, F. A. B. Coutinho, K. Goh, L. F. Lopez, S. Ma, and E. Massad (2008). Modelling the control strategies against dengue in Singapore. *Epidemiology and Infection 136*(3), 309–319.

Cairns, A. J. G., D. Blake, and K. Dowd (2006). A two-factor model for stochastic mortality with parameter uncertainty: Theory and calibration. *Journal of Risk and Insurance 73*(4), 687–718.

Catching, A., S. Capponi, M. T. Yeh, S. Bianco, and R. Andino (2021). Examining the interplay between face mask usage, asymptomatic transmission, and social distancing on the spread of covid-19. *Scientific Reports 11*(1).

Chanprasopchai, P., I. M. Tang, and P. Pongsumpun (2018). SIR model for dengue disease with effect of dengue vaccination. *Computational and Mathematical Methods in Medicine 2018*.

Charpentier, A. (2008). Insurability of climate risks. *The Geneva Papers on Risk and Insurance - Issues and Practice 33*(1), 91–109.

Chen, Z., Y. Lu, J. Zhang, and W. Zhu (2023). Managing weather risk with a neural network-based index insurance. *Management Science, forthcoming*.

Collins, S. (2020). Insurers wary of meeting growing demand for specialist pandemic cover. https://www.commercialriskonline.com/insurers-wary-meeting-growing-demand-specialist-pandemic-cover/. Accessed November 18, 2020.

Costa, A. O. C., H. d. C. A. Neto, A. P. L. Nunes, R. D. de Castro, and R. N. de Almeida (2021). COVID-19: Is reinfection possible? *EXCLI Journal 20*, 522–536.

Coutinho, F. A. B., M. N. Burattini, L. F. Lopez, and E. Massad (2005). An approximate threshold condition for non-autonomous system: An application to a vector-borne infection. *Mathematics and Computers in simulation 70*(3), 149–158.

Coutinho, F. A. B., M. N. Burattini, L. F. Lopez, and E. Massad (2006). Threshold conditions for a non-autonomous epidemic system describing the population dynamics of dengue. *Bulletin of Mathematical Biology 68*(8), 2263–2282.

Cowley, A. and J. D. Cummins (2005). Securitization of life insurance assets and liabilities. *Journal of Risk and Insurance 72*(2), 193–226.

Cummins, J. D. (2006). Should the government provide insurance for catastrophes? *Federal Reserve Bank of St. Louis Review 88*(4), 337–380.

Cummins, J. D. (2008). Cat bonds and other risk-linked securities: State of the market and recent developments. *Risk Management and Insurance Review 11*(1), 23–47.

Cummins, J. D., N. Doherty, and A. Lo (2002). Can insurers pay for the "big one"? measuring the capacity of the insurance market to respond to catastrophic losses. *Journal of Banking & Finance 26*(2), 557–583.

Cummins, J. D., D. Lalonde, and R. D. Phillips (2004). The basis risk of catastrophic-loss index securities. *Journal of Financial Economics 71*(1), 77–111.

Cummins, J. D. and P. Trainar (2009). Securitization, insurance, and reinsurance. *The Journal of Risk and Insurance 76*(3), 463–492.

Cummins, J. D. and M. A. Weiss (2009). Convergence of insurance and financial markets: Hybrid and securitized risk-transfer solutions. *Journal of Risk and Insurance 76*(3), 493–545.

De la Sen, M. and A. Ibeas (2021). On an SE(Is)(Ih)AR epidemic model with combined vaccination and antiviral controls for covid-19 pandemic. *Advances in Difference Equations 2021*, 92.

Denuit, M., P. Devolder, and A.-C. Goderniaux (2007). Securitization of longevity risk: Pricing survivor bonds with Wang transform in the Lee-Carter framework. *Journal of Risk and Insurance 74*(1), 87–113.

Derouich, M. and A. Boutayeb (2006). Dengue fever: Mathematical modelling and computer simulation. *Applied Mathematics and Computation 177*(2), 528–544.

Doherty, N. A. (1997). Financial innovation in the management of catastrophe risk. *Journal of Applied Corporate Finance 10*(3), 84–95.

Dowd, K., D. Blake, A. J. Cairns, and P. Dawson (2006). Survivor swaps. *Journal of Risk and Insurance 73*(1), 1–17.

Eggink, D., S. P. Andeweg, H. Vennema, N. van Maarseveen, K. Vermaas, B. Vlaemynck, R. Schepers, A. B. van Gageldonk-Lafeber, S. van den Hof, C. B. Reusken, and M. J. Knol (2021). Increased risk of infection with sars-cov-2 omicron compared to delta in vaccinated and previously infected individuals, the netherlands, 22 november to 19 december 2021. *medRxiv*.

Eletreby, R., Y. Zhuang, K. M. Carley, O. Yağan, and H. V. Poor (2020). The effects of evolutionary adaptations on spreading processes in complex networks. *Proceedings of the National Academy of Sciences 117*(11), 5664–5670.

Falahi, S. and A. Kenarkoohi (2020). COVID-19 reinfection: prolonged shedding or true reinfection? *New Microbes and New Infections 38*, 100812.

Feng, R. and J. Garrido (2011). Actuarial applications of epidemiological models. *North American Actuarial Journal 15*(1), 112–136.

Finken, S. and C. Laux (2009). Catastrophe bonds and reinsurance: The competitive effect of information-insensitive triggers. *Journal of Risk and Insurance 76*(3), 579–605.

Fouque, F., R. Carinci, P. Gaborit, J. Issaly, D. J. Bicout, and P. Sabatier (2006). Aedes aegypti survival and dengue transmission patterns in French Guiana. *Journal of Vector Ecology 31*(2), 390–399.

Froot, K. A. (2001). The market for catastrophe risk: A clinical examination. *Journal of Financial Economics 60*(2-3), 529–571.

Giordano, G., F. Blanchini, R. Bruno, P. Colaneri, A. D. Filippo, A. D. Matteo, and M. Colaneri (2020). Modelling the COVID-19 epidemic and implementation of population-wide interventions in Italy. *Nature Medicine 26*, 855—860.

Gousseff, M., P. Penot, L. Gallay, D. Batisse, N. Benech, K. Bouiller, R. Collarino, A. Conrad, D. Slama, C. Joseph, A. Lemaignen, F.-X. Lescure, B. Levy, M. Mahevas, B. Pozzetto, N. Vignier, B. Wyplosz, D. Salmon, F. Goehringer, and E. Botelho-Nevers (2020). Clinical recurrences of covid-19 symptoms after recovery: Viral relapse, reinfection or inflammatory rebound? *Journal of Infection 81*(5), 816–846.

Gründl, H., D. Guxha, A. Kartasheva, and H. Schmeiser (2021). Insurability of pandemic risks. *Journal of Risk and Insurance 88*(4), 863–902.

Halstead, S. B. (2007). Dengue. *Lancet 370*(9599), 1644–1652.

Härdle, W. K. and B. L. Cabrera (2010). Calibrating CAT bonds for Mexican earthquakes. *Journal of Risk and Insurance 77*(3), 625–650.

Hartwig, R., G. Niehaus, and J. Qiu (2020). Insurance for economic losses caused by pandemics. *The Geneva Risk and Insurance Review 45*(2), 134–170.

Hilsenrath, J. (2020). Global viral outbreaks like coronavirus, once rare, will become more common. https://www.wsj.com/articles/viral-outbreaks-once-rare-become-part-of-the-global-landscape-11583455309. Accessed: November 23, 2020.

Huang, S., J. Zhang, and W. Zhu (2023). Storm cat bond: Modeling and valuation. *North American Actuarial Journal, forthcoming*.

International Bank for Reconstruction and Development (2017a). Pandemic emergency financing facility. https://www.worldbank.org/en/topic/pandemics/brief/pandemic-emergency-financing-facility. Accessed: November 23, 2020.

International Bank for Reconstruction and Development (2017b). Prospectus supplement dated June 28, 2017. http://pubdocs.worldbank.org/en/882831509568634367/PEF-Final-Prospectus-PEF.pdf. Accessed: November 23, 2020.

International Bank for Reconstruction and Development (2020). Population, total - Singapore. https://data.worldbank.org/indicator/SP.POP.TOTL?locations=SG. Accessed: November 29, 2020.

International Monetary Fund (2020). The great lockdown: Worst economic downturn since the great depression. https://blogs.imf.org/2020/04/14/the-great-lockdown-worst-economic-downturn-since-the-great-depression/. Accessed: November 23, 2020.

Ito, H., J. Ai, and A. Ozawa (2016). Managing weather risks: The case of J. League soccer teams in Japan. *Journal of Risk and Insurance 83*(4), 877–912.

Jia, N. and L. Tsui (2005). Epidemic modelling using SARS as a case study. *North American Actuarial Journal 9*(4), 28–42.

Johns Hopkins (2022). Johns hopkins coronavirus resource center. `https://github.com/CSSEGISandData/COVID-19/tree/master/csse_covid_19_data/csse_covid_19_time_series`. Accessed: July 2, 2022.

Johns Hopkins CRC (2022). Mortality analyses by Johns Hopkins Coronavirus Resource Center. `https://coronavirus.jhu.edu/data/mortality`. Accessed: Feb 16, 2022.

Kang, H., Y. Wang, Z. Tong, and X. Liu (2020). Retest positive for sars-cov-2 rna of "recovered" patients with covid-19: Persistence, sampling issues, or re-infection? *Journal of Medical Virology 92*(11), 2263–2265.

Karim, S. S. and Q. A. Karim (2021). Omicron sars-cov-2 variant: A new chapter in the covid-19 pandemic. *The Lancet 398*(10317), 2126–2128.

Kermack, W. O. and A. G. McKendrick (1927). A contribution to the mathematical theory of epidemics. *Proceedings of the Royal Society of London 115*(772), 700–721.

Kwon, S., A. D. Joshi, C.-H. Lo, D. A. Drew, L. H. Nguyen, C.-G. Guo, W. Ma, R. S. Mehta, F. M. Shebl, E. T. Warner, and et al. (2021). Association of social distancing and face mask use with risk of covid-19. *Nature Communications 12*(1).

Li, J. S.-H., W.-S. Chan, and R. Zhou (2017). Semicoherent multipopulation mortality modeling: The impact on longevity risk securitization. *Journal of Risk and Insurance 84*(3), 1025–1065.

Lin, Q., S. Zhao, D. Gao, Y. Lou, S. Yang, S. S. Musa, M. H. Wang, Y. Cai, W. Wang, L. Yang, and D. He (2020). A conceptual model for the coronavirus disease 2019 (COVID-19) outbreak in Wuhan, China with individual reaction and governmental action. *International Journal of Infectious Diseases 93*, 211–216.

Lin, Y. and S. H. Cox (2005). Securitization of mortality risks in life annuities. *Journal of Risk and Insurance 72*(2), 227–252.

Lin, Y. and S. H. Cox (2007). Natural hedging of life and annuity mortality risks. *North American Actuarial Journal 11*(3), 1–15.

Linka, K., M. Peirlinck, and E. Kuhl (2020). The reproduction number of COVID-19 and its correlation with public health interventions. *Computational Mechanics 66*(4), 1035–1050.

Liu, Y., A. A. Gayle, A. Wilder-Smith, and J. Rocklöv (2020, 02). The reproductive number of COVID-19 is higher compared to SARS coronavirus. *Journal of Travel Medicine 27*(2). taaa021.

Lloyd's (2020). Supporting global recovery and resilience for customers and economies. https://www.lloyds.com/news-and-risk-insight/coronavirus-updates-hub/supporting-global-recovery-and-resilience-for-customers-and-economies. Accessed: November 23, 2020.

MacMinn, R. and A. Richter (2018). The choice of trigger in an insurance linked security: The mortality risk case. *Insurance: Mathematics and Economics 78*, 174–182.

Malkov, E. (2020). Simulation of coronavirus disease 2019 (COVID-19) scenarios with possibility of reinfection. *Chaos, Solitons and Fractals 139*, 110296.

Maurício de Carvalho, J. P. and B. Moreira-Pinto (2021). A fractional-order model for COVID-19 dynamics with reinfection and the importance of quarantine. *Chaos, Solitons and Fractals 151*.

McKinsey & Company (2021). The impact of covid-19 on capital markets, one year in. *McKinsey & Company*.

Ministry of Health Singapore (2019). Weekly number of dengue and dengue haemorrhagic fever cases. https://data.gov.sg/dataset/weekly-number-of-dengue-and-dengue-haemorrhagic-fever-cases. Accessed: November 29, 2020.

Ministry of Health Singapore (2020). Population and vital statistics. https://www.moh.gov.sg/resources-statistics/singapore-health-facts/population-and-vital-statistics. Accessed: November 29, 2020.

National Environment Agency Singapore (2020). Dengue cases. https://www.nea.gov.sg/dengue-zika/dengue/dengue-cases. Accessed: November 29, 2020.

Newton, E. A. and P. Reiter (1992). A model of the transmission of dengue fever with an evaluation of the impact of ultra-low volume (ULV) insecticide applications on dengue epidemics. *American Journal of Tropical Medicine and Hygiene 47*(6), 709–720.

Niehaus, G. (2002). The allocation of catastrophe risk. *Journal of Banking & Finance 26*, 585–596.

Ooi, E.-E., K.-T. Goh, and D. J. Gubler (2006). Dengue prevention and 35 years of vector control in Singapore. *Emerging Infectious Diseases 12*(6), 887–893.

Ooi, E. E., T. J. Hart, H. C. Tan, and S. H. Chan (2001). Dengue seroepidemiology in Singapore. *Lancet 357*(9257), 685–686.

Organisation for Economic Co-operation and Development (2020). Responding to the COVID-19 and pandemic protection gap in insurance. https://www.oecd.org/coronavirus/policy-responses/responding-to-the-covid-19-and-pandemic-protection-gap-in-insurance-35e74736/. Accessed November 18, 2020.

Park, M., A. R. Cook, J. T. Lim, Y. Sun, and B. L. Dickens (2020). A systematic review of COVID-19 epidemiology based on current evidence. *Journal of Clinical Medicine 9*(4).

Perera, S. S. N. (2019). Insurance model to estimate the financial risk due to direct medical cost on dengue outbreaks. In *Mathematics Applied to Engineering, Modelling, and Social Issues*, pp. 629–663. Springer International Publishing.

Polacek, A. et al. (2018). Catastrophe bonds: A primer and retrospective. *Chicago Fed Letter 405*, 1–7.

Rajarethinam, J., L.-W. Ang, J. Ong, J. Ycasas, H. C. Hapuarachchi, G. Yap, C.-S. Chong, Y.-L. Lai, J. Cutter, D. Ho, V. Lee, and L.-C. Ng (2018). Dengue in Singapore from 2004 to 2016: Cyclical epidemic patterns dominated by serotypes 1 and 2. *The American Journal of Tropical Medicine and Hygiene 99*(1), 204–210.

Raza, A., M. S. Arif, and M. Rafiq (2019). A reliable numerical analysis for stochastic dengue epidemic model with incubation period of virus. *Advances in Difference Equations 32*.

Richter, A. and T. C. Wilson (2020). COVID-19: Implications for insurer risk management and the insurability of pandemic risk. *The Geneva Risk and Insurance Review 45*, 171–199.

Rigau-Pérez, J. G., G. G. Clark, D. J. Gubler, P. Reiter, E. J. Sanders, and A. V. Vorndam (1998). Dengue and dengue haemorrhagic fever. *Lancet 352*(9132), 971–977.

Scott, T. W., P. H. Amerasinghe, A. C. Morrison, L. H. Lorenz, G. G. Clark, D. Strickman, P. Kittayapong, and J. D. Edman (2000). Longitudinal studies of Aedes aegypti (Diptera: Culicidae) in Thailand and Puerto Rico: Blood feeding frequency. *Journal of Medical Entomology 37*(1), 89–101.

Sridhar, A., O. Yağan, R. Eletreby, S. A. Levin, J. B. Plotkin, and H. V. Poor (2021). Leveraging a multiple-strain model with mutations in analyzing the spread of covid-19. In *ICASSP 2021 - 2021 IEEE International Conference on Acoustics, Speech and Signal Processing (ICASSP)*, pp. 8163–8167.

Swiss Re (2021, 08). Insurance-Linked Securities Market Insights. Technical report, Swiss Re.

Tan, K. S., C. Weng, and J. Zhang (2022). Optimal dynamic longevity hedge with basis risk. *European Journal of Operational Research 297*(1), 325–337.

Tao, W., X. Wang, G. Zhang, M. Guo, H. Ma, D. Zhao, Y. Sun, J. He, L. Liu, K. Zhang, Y. Wang, J. Weng, X. Ma, T. Jin, and S. Zhu (2021). Re-detectable positive sars-cov-2 rna tests in patients who recovered from covid-19 with intestinal infection. *Protein & Cell 12*(3), 230–235.

Townsend, J. P., H. B. Hassler, Z. Wang, S. Miura, J. Singh, S. Kumar, N. H. Ruddle, A. P. Galvani, and A. Dornburg (2021). The durability of immunity against reinfection by sars-cov-2: A comparative evolutionary study. *The Lancet Microbe 2*(12), E666–E675.

Wang, S. (1996). Premium calculation by transforming the layer premium density. *ASTIN Bulletin: The Journal of the IAA 26*(1), 71–92.

Wang, S. (2000). A class of distortion operators for pricing financial and insurance risks. *Journal of Risk and Insurance 67*(1), 15–36.

Wang, S. S. (2002). A universal framework for pricing financial and insurance risks. *ASTIN Bulletin: The Journal of the IAA 32*(2), 213–234.

Wang, Y., H. Tian, L. Zhang, M. Zhang, D. Guo, W. Wu, X. Zhang, G. L. Kan, L. Jia, D. Huo, B. Liu, X. Wang, Y. Sun, Q. Wang, P. Yang, and C. R. MacIntyre (2020). Reduction of secondary transmission of sars-cov-2 in households by face mask use, disinfection and social distancing: a cohort study in beijing, china. *BMJ Global Health 5*(5).

Woodard, J. D. and P. Garcia (2008). Weather derivatives, spatial aggregation, and systemic risk: Implications for reinsurance hedging. *Journal of Agricultural and Resource Economics 33*(1), 34–51.

World Bank (2020). United States population, total. https://data.worldbank.org/country/united-states?view=chart. Accessed: December 29, 2021.

World Health Organization (2017). Dengue explorer. https://ntdhq.shinyapps.io/dengue5/. Accessed: November 29, 2020.

Zhai, S., G. Luo, T. Huang, X. Wang, J. Tao, and P. Zhou (2021). Vaccination control of an epidemic model with time delay and its application to covid-19. *Nonlinear Dynamics 106*, 1279–1292.

Zhang, J., K. S. Tan, and C. Weng (2019). Index insurance design. *ASTIN Bulletin: The Journal of the IAA 49*(2), 491–523.

Zhu, W., K. S. Tan, L. Porth, and C.-W. Wang (2018). Spatial dependence and aggregation in weather risk hedging: a lévy subordinated hierarchical archimedean copulas (lshac) approach. *ASTIN Bulletin: The Journal of the IAA 48*(2), 779–815.

Zhu, W., K. S. Tan, and C.-W. Wang (2017). Modeling multicountry longevity risk with mortality dependence: A lévy subordinated hierarchical archimedean copulas approach. *Journal of Risk and Insurance 84*(S1), 477–493.

Online Appendix

A Other Pandemic Bond Structures

In addition to the binary reduction designs outlined in Section 3.1.1, in this appendix we consider some other pandemic bond design structures. For example, linear reduction design for coupons and/or principal payouts can be considered. Let x and y be trigger levels defined in Table 1, $x+c_1$ be the trigger that coupon reduces to zero in linear coupon design, and $y+c_2$ be the trigger that the principal payout reduces to zero in linear principal design.

Linear Coupon and Fixed Principal (LCFP)

In a LCFP structure, the bond pays investors a fixed principal value of f upon bond maturity. Different from BCFP's binary type of coupon reduction, in LCFP, the coupon payout reduces linearly after $RC_t^{(p)}$ reaches the trigger level. In particular, investors are paid the full annual coupon amount of b if the rolling cases do not exceed the fixed trigger level x at all time during the year, i.e., $RC_t^{(p)} < x$. At any time during the year, if the rolling cases fall in the interval of $[x, x+c_1]$, B_t will be reduced contingent on the value of $RC_t^{(p)}$, in a linear way. B_t is zero for $RC_t^{(p)}$ above level $x+c_1$. More specifically, coupon payout in period t is

$$B_t = \begin{cases} 0, & \text{if } RC_t^{(p)} \geq x + c_1, \\ \frac{b}{c_1}(x + c_1 - RC_t^{(p)}), & \text{if } x \leq RC_t^{(p)} < x + c_1, \\ b, & \text{if } RC_t^{(p)} < x. \end{cases} \tag{A.1}$$

Linear Coupon and Binary Principal (LCBP)

In a LCBP design, we introduce a linear reduction structure in the coupon payout after $RC_t^{(p)}$ reaches the trigger level. The principal payout is the same as BCBP, expressed in Equation (3). The coupon payout in period t is

$$B_t = \begin{cases} 0, & \text{if } \max\limits_{1\leq s\leq t}\{RC_s^{(p)}\} \geq y \text{ or } x + c_1 \leq RC_t^{(p)} < y, \\ \frac{b}{c_1}(x + c_1 - RC_t^{(p)}), & \text{if } \max\limits_{1\leq s\leq t-1}\{RC_s^{(p)}\} < y \text{ and } x \leq RC_t^{(p)} < x + c_1, \\ b, & \text{if } \max\limits_{1\leq s\leq t-1}\{RC_s^{(p)}\} < y \text{ and } RC_t^{(p)} < x, \end{cases} \tag{A.2}$$

where we assume $x + c_1 \leq y$.

Linear Coupon and Linear Principal (LCLP)

A LCLP structure is similar to LCBP except that the principal payout decreases linearly after the second layer y is triggered. Therefore, its coupon payment, B_t, follows Equation (A.2), and principal payout upon maturity is

$$F = \begin{cases} 0, & \text{if } \max\limits_{1\le t\le n}\{RC_t^{(p)}\} > y + c_2, \\ \frac{f}{c_2}(y + c_2 - RC_t^{(p)}), & \text{if } y < \max\limits_{1\le t\le n}\{RC_t^{(p)}\} \le y + c_2, \\ f, & \text{if } \max\limits_{1\le t\le n}\{RC_t^{(p)}\} \le y. \end{cases} \tag{A.3}$$

Fixed Coupon Binary Principal (FCBP)

In addition to all previous designs with variable coupons, we also consider a fixed coupon design with variable principal. One example is a fixed coupon binary principal (FCBP) design. This design is rarely seen in practice, since coupon payouts are usually ceased once principal payout is triggered, but bond issuers may consider this design in the future. An FCBP design can be seen as a special version of annuities, so investors who desire guaranteed periodic returns might be interested in such a product. The coupon payouts are guaranteed with the maximum value, b, while the principal payout upon maturity is defined in Equation (3).

Table A.1 shows the summary of the coronavirus bond coupon rates of all six designs. Both binary reduction and linear reduction of coupon and/or principal payouts are considered. Table A.2 shows the summary of the bond average return for the coronavirus bond for the six designs. We can see linear reduction designs have lower coupon rates and lower average bond returns than binary reduction designs, all else held equal, i.e., LCFP < BCFP and LCLP < LCBP < BCBP. This is expected because under linear reduction designs, the coupon or principal payouts could still have some positive values when the trigger levels x or y are reached. Nevertheless, the difference between binary reduction designs and linear reduction designs is very small compared to the difference between FP and VP designs. For example, the largest difference in the coupon rates between LCLP and BCBP is only 0.301% at $\lambda_3 = 0.45$, interest rate 1%, and $x/N = 0.0001\%$, whereas the difference between BCFP and BCBP is 8.992% for the same set of parameters. Moreover, among FCBP, BCBP, and LCBP which all have binary principal designs, Design FCBP has the lowest coupon rates, i.e., FCBP < LCBP < BCBP. This is expected because a fixed coupon design guarantees coupon payouts, leading to lower investment risks. Nonetheless, the coupon rates of FCBP are still much higher than those with fixed principal designs.

Table A.1: Coronavirus Bond Coupon Rate Summary (in %)

Interest rate		1%			2%			3%	
x/N (%)	0.0001	0.01	1	0.0001	0.01	1	0.0001	0.01	1
y/N (%)	0.001	0.1	10	0.001	0.1	10	0.001	0.1	10
Panel A: Design Binary Coupon and Fixed Principal (BCFP)									
CB $\lambda_0 = 0$	1.043	1.029	1.019	2.085	2.058	2.039	3.127	3.086	3.058
CB $\lambda_1 = 0.05$	1.048	1.032	1.022	2.095	2.065	2.044	3.142	3.097	3.065
CB $\lambda_2 = 0.25$	1.073	1.051	1.035	2.145	2.101	2.070	3.217	3.151	3.105
CB $\lambda_3 = 0.45$	1.108	1.077	1.055	2.216	2.154	2.109	3.324	3.231	3.163
Panel B: Design Liner Coupon and Fixed Principal (LCFP)									
CB $\lambda_0 = 0$	1.041	1.027	1.017	2.081	2.054	2.035	3.121	3.081	3.052
CB $\lambda_1 = 0.05$	1.045	1.030	1.020	2.090	2.061	2.039	3.135	3.091	3.058
CB $\lambda_2 = 0.25$	1.069	1.047	1.031	2.138	2.095	2.063	3.207	3.142	3.094
CB $\lambda_3 = 0.45$	1.103	1.072	1.049	2.205	2.144	2.097	3.308	3.216	3.146
Panel C: Design Binary Coupon and Binary Principal (BCBP)									
CB $\lambda_0 = 0$	4.483	3.349	2.557	5.519	4.374	3.574	6.555	5.399	4.591
CB $\lambda_1 = 0.05$	4.902	3.649	2.767	5.943	4.677	3.787	6.983	5.705	4.806
CB $\lambda_2 = 0.25$	7.048	5.206	3.879	8.109	6.250	4.911	9.170	7.294	5.942
CB $\lambda_3 = 0.45$	10.132	7.496	5.554	11.224	8.563	6.603	12.316	9.630	7.652
Panel D: Design Linear Coupon and Binary Principal (LCBP)									
CB $\lambda_0 = 0$	4.476	3.345	2.555	5.511	4.369	3.571	6.546	5.393	4.587
CB $\lambda_1 = 0.05$	4.895	3.645	2.765	5.934	4.672	3.783	6.972	5.699	4.802
CB $\lambda_2 = 0.25$	7.033	5.198	3.874	8.092	6.240	4.904	9.151	7.283	5.934
CB $\lambda_3 = 0.45$	10.103	7.479	5.543	11.192	8.544	6.590	12.280	9.609	7.636
Panel E: Design Linear Coupon and Linear Principal (LCLP)									
CB $\lambda_0 = 0$	4.373	3.277	2.471	5.409	4.302	3.488	6.444	5.326	4.505
CB $\lambda_1 = 0.05$	4.779	3.568	2.670	5.819	4.596	3.689	6.859	5.623	4.709
CB $\lambda_2 = 0.25$	6.853	5.076	3.719	7.915	6.119	4.751	8.976	7.163	5.782
CB $\lambda_3 = 0.45$	9.833	7.291	5.298	10.924	8.358	6.348	12.015	9.424	7.397
Panel F: Design Fixed Coupon and Binary Principal (FCBP)									
CB $\lambda_0 = 0$	4.184	3.194	2.476	5.153	4.172	3.461	6.121	5.151	4.447
CB $\lambda_0 = 0.05$	4.540	3.459	2.668	5.504	4.435	3.652	6.470	5.411	4.636
CB $\lambda_0 = 0.25$	6.270	4.790	3.659	7.218	5.752	4.632	8.166	6.715	5.607
CB $\lambda_0 = 0.45$	8.529	6.608	5.071	9.454	7.552	6.031	10.380	8.498	6.991

Note: This table summarizes coupon rates for a 3-year coronavirus bond with face value \$1,000 sold at par.

Table A.2: The Bond Average Return r_{avg} (in %) for a 3-year coronavirus bond with face value \$1,000 sold at par estimated based on Equation (8)

Interest rate		1%			2%			3%	
x/N (%)	0.0001	0.01	1	0.0001	0.01	1	0.0001	0.01	1
y/N (%)	0.001	0.1	10	0.001	0.1	10	0.001	0.1	10
Panel A: Design Binary Coupon and Fixed Principal (BCFP)									
CB $\lambda_0 = 0$	1.001	1.001	1.001	2.000	2.000	2.000	3.000	3.000	3.000
CB $\lambda_1 = 0.05$	1.006	1.004	1.003	2.009	2.007	2.005	3.014	3.010	3.007
CB $\lambda_2 = 0.25$	1.030	1.022	1.016	2.058	2.042	2.031	3.086	3.064	3.046
CB $\lambda_3 = 0.45$	1.064	1.048	1.036	2.126	2.094	2.069	3.189	3.141	3.104
Panel B: Design Linear Coupon and Fixed Principal (LCFP)									
CB $\lambda_0 = 0$	1.001	1.001	1.001	2.000	2.000	2.000	3.000	3.000	3.000
CB $\lambda_1 = 0.05$	1.005	1.004	1.003	2.009	2.006	2.004	3.014	3.010	3.007
CB $\lambda_2 = 0.25$	1.028	1.021	1.015	2.055	2.040	2.028	3.082	3.060	3.041
CB $\lambda_3 = 0.45$	1.061	1.045	1.032	2.120	2.088	2.062	3.179	3.132	3.093
Panel C: Design Binary Coupon and Binary Principal (BCBP)									
CB $\lambda_0 = 0$	1.001	1.001	1.001	2.000	2.000	2.000	3.000	3.000	3.000
CB $\lambda_1 = 0.05$	1.408	1.295	1.209	2.409	2.296	2.209	3.413	3.299	3.211
CB $\lambda_2 = 0.25$	3.476	2.812	2.300	4.501	3.831	3.314	5.525	4.849	4.328
CB $\lambda_3 = 0.45$	6.454	5.046	3.947	7.508	6.087	4.978	8.561	7.128	6.009
Panel D: Design Linear Coupon and Binary Principal (LCBP)									
CB $\lambda_0 = 0$	1.001	1.001	1.001	2.000	2.000	2.000	3.000	3.000	3.000
CB $\lambda_1 = 0.05$	1.407	1.294	1.208	2.409	2.295	2.209	3.413	3.298	3.211
CB $\lambda_2 = 0.25$	3.471	2.809	2.298	4.495	3.827	3.311	5.519	4.845	4.325
CB $\lambda_3 = 0.45$	6.440	5.037	3.940	7.492	6.077	4.970	8.543	7.117	6.000
Panel E: Design Linear Coupon and Linear Principal (LCLP)									
CB $\lambda_0 = 0$	1.082	1.058	1.001	2.080	2.056	2.000	3.080	3.056	3.000
CB $\lambda_1 = 0.05$	1.476	1.342	1.197	2.476	2.343	2.198	3.480	3.345	3.200
CB $\lambda_2 = 0.25$	3.474	2.811	2.227	4.498	3.829	3.241	5.522	4.847	4.255
CB $\lambda_3 = 0.45$	6.349	4.972	3.780	7.403	6.012	4.811	8.455	7.053	5.843
Panel F: Design Fixed Coupon and Binary Principal (FCBP)									
CB $\lambda_0 = 0$	1.001	1.001	1.001	2.000	2.000	2.000	3.000	3.000	3.000
CB $\lambda_1 = 0.05$	1.369	1.273	1.197	2.363	2.269	2.193	3.360	3.266	3.192
CB $\lambda_1 = 0.25$	3.153	2.632	2.200	4.131	3.615	3.188	5.109	4.599	4.176
CB $\lambda_1 = 0.05$	5.482	4.489	3.633	6.436	5.453	4.606	7.390	6.418	5.580